TN TDOT Department of Transportation

U.S. Department of Transportation
Federal Highway Administration

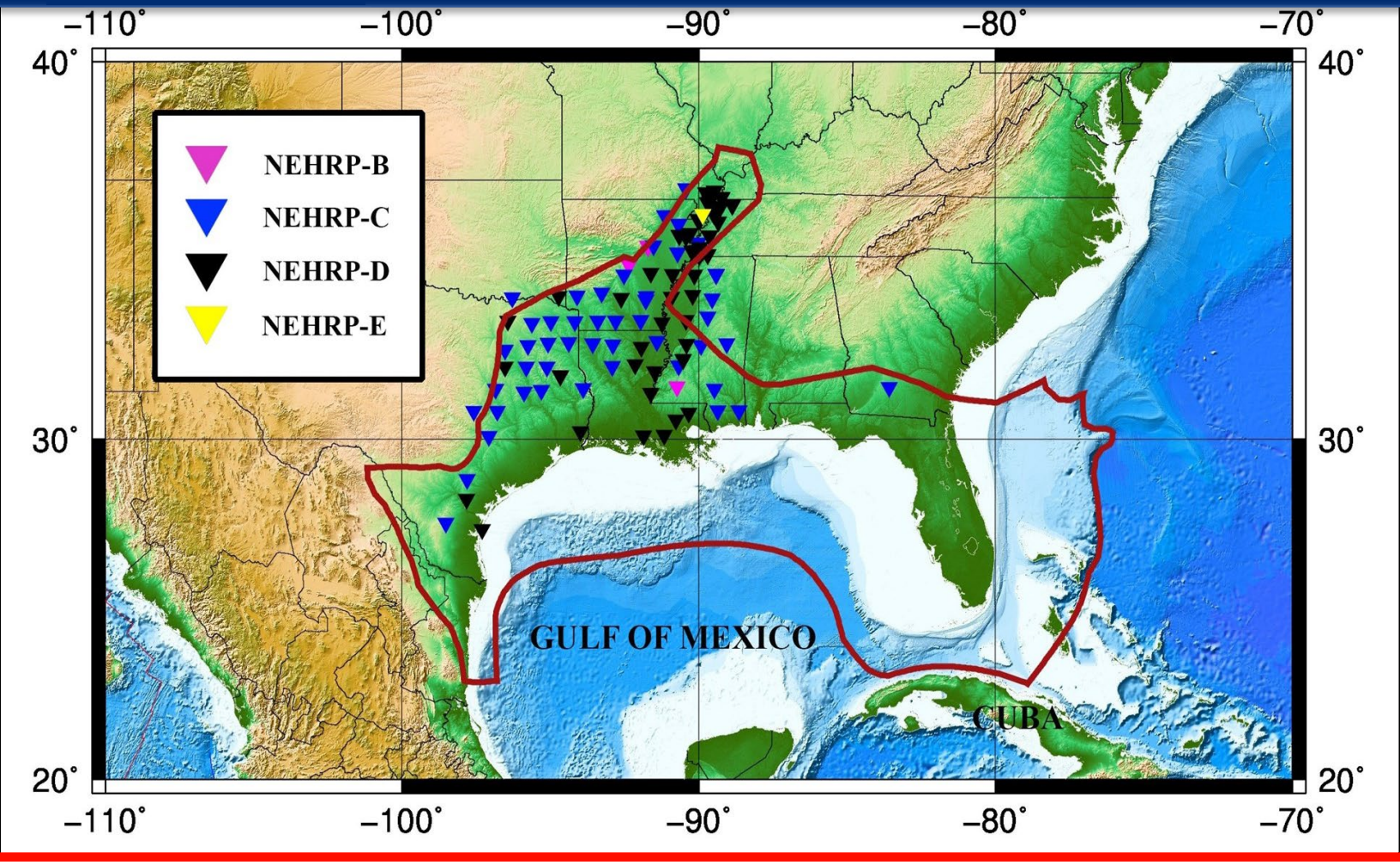

The Estimation of Seismic Parameters for Updating Ground Motion Models for Central and Eastern United States

Research Final Report from The University of Memphis | Shahram Pezeshk and Christie Assadollahi| February 28, 2022

Sponsored by Tennessee Department of Transportation Long Range Planning Research Office & Federal Highways Administration

THE UNIVERSITY OF MEMPHIS

DISCLAIMER

This research was funded through the State Planning and Research (SPR) Program by the Tennessee Department of Transportation and the Federal Highway Administration under RES2020-25*: The Estimation of Seismic Parameters for Updating Ground Motion Models for Central and Eastern United States* **.**

Technical Report Documentation Page

1. Report No. RES2020-25	2. Government Accession No.	3. Recipient's Catalog No.
4. Title and Subtitle *The Estimation of Seismic Parameters for Updating Ground Motion Models for Central and Eastern United States*		5. Report Date February 29, 2022 6. Performing Organization Code
7. Author(s) Shahram Pezeshk and Christie Moore		8. Performing Organization Report No.
9. Performing Organization Name and Address Department of Civil Engineering The University of Memphis Memphis, TN 38152		10. Work Unit No. (TRAIS) 11. Contract or Grant No.
12. Sponsoring Agency Name and Address Tennessee Department of Transportation 505 Deaderick Street, Suite 900 Nashville, TN 37243		13. Type of Report and Period Covered Final Report 08/01/2019 to 02/28/2022 14. Sponsoring Agency Code
15. Supplementary Notes Conducted in cooperation with the U.S. Department of Transportation, Federal Highway Administration.		

16. Abstract

The main objective of this study was to determine seismological parameters in Central and Eastern North America (CENA), including constraints on the geometrical spreading, anelastic attenuation, stress parameters, and site attenuation parameters (kappa). To determine the seismological parameters, the recently developed and published Ground Motion Models (GMMs) for the NGA-East were used. In addition to the main objective, as part of this study, three new ground-motion models (GMMs) were developed: (1) a new model for vertical to horizontal response spectral ratios for central and eastern North America; (2) a ground-motion prediction model for small-to-moderate induced earthquakes for central and eastern United States; and (3) a ground motion model for the Gulf Coast region of the United States, which includes part of West Tennessee. These three GMMs are presented as supplementary material to this report

We used a genetic algorithm (GA) to invert weighted geometric mean estimates of horizontal response-spectral acceleration from the empirical NGA-East ground-motion models to successfully estimate a consistent set of seismological parameters that can be used along with an equivalent point-source stochastic model to mimic the general scaling characteristics of these ground-motion models. The inversion is performed for events of **M** 4 – 8.0, R_{RUP} = 1 to 300 km, T = 0.01 – 10 sec (f = 0.1 – 10 Hz).

This study is the first to perform a formal inversion using the extensive and peer-reviewed CENA GMMs developed for the NGA-East project and using a formal GA approach. The approach was validated by using simulated small-to-moderate magnitude and large-magnitude data derived from the NGA-West2 GMMs (Zandieh *et al*., 2016, 2018; Pezeshk *et al.*, 2015).

17. Key Words **Ground Motion Model, Seismological Parameters, Attenuation Parameters, GMMs, NGA East Region**	18. Distribution Statement No restriction. This document is available to the public from the sponsoring agency at the website http://www.tn.gov/		
19. Security Classif. (of this report) Unclassified	20. Security Classif. (of this page) Unclassified	21. No. of Pages 58	22. Price TBD

Acknowledgment

The author would like to thank Mr. Ted Kniazewycz, Ms. Melanie Murphy, and Ms. Allison Gwinup for their support of this project.

Executive Summary

The main objective of this study was to determine seismological parameters in Central and Eastern North America (CENA), including constraints on the geometrical spreading, anelastic attenuation, stress parameter, and site attenuation parameters (kappa). To determine the seismological parameters, the recently developed and published Ground Motion Models (GMMs) for the NGA-East were used. In addition to the main objective, as part of this study, three new ground-motion models (GMMs) were developed: (1) a new model for vertical to horizontal response spectral ratios for central and eastern North America; (2) a ground-motion prediction model for small-to-moderate induced earthquakes for central and eastern United States; and (3) A Ground motion model for the Gulf Coast region of the United States, which includes part of West Tennessee. These three GMMs are presented as supplementary material to this report.

We used a genetic algorithm (GA) to determine the weighted geometric mean estimates of horizontal response-spectral acceleration from the empirical NGA-East ground-motion models to successfully estimate a consistent set of seismological parameters that can be used along with an equivalent point-source stochastic model to mimic the general scaling characteristics of these ground-motion models. The process of finding the seismological parameters from GMMs is referred to as an "inversion." The inversion is performed for events of **M** 4 – 8.0, R_{RUP} = 1 to 300 km, T = 0.01 – 10 sec (f = 0.1 – 10 Hz).

This study is the first to perform a formal inversion using the extensive and peer-reviewed CENA GMMs developed for the NGA-East project and using a formal GA approach. The approach was validated by using simulated small-to-moderate magnitude and large-magnitude data derived from the NGA-West2 GMMs (Zandieh *et al*., 2016, 2018; Pezeshk *et al.*, 2015).

Key Findings

This study developed or determined:

- Seismological parameters needed to update Ground Motion Models for Central and Eastern United States.
- Seismological parameters that are well correlated and most appropriate for use for the Central United States.
- A new model for vertical to horizontal response spectral ratios for Central and Eastern North America.
- A Ground-motion prediction model for small-to-moderate induced earthquakes for Central and Eastern United States.
- A Ground motion model for the Gulf Coast region of the United States, which includes part of West Tennessee.

Key Recommendations

It is important to note that it has been 10 years since ground-motion models (GMMs) for the Central United States have been developed. Since then, and since the publication of NGA-EAST GMMs (PEER, 2015), there have been various advancements in site response for the Central and Eastern North America (CENA), but there has not been any new research to improve the

seismological parameters for CENA. This research will provide the much-needed information for updating GMMs developed as part of NGA-East in 2015.

The improved seismological parameters will have a significant and far-reaching effect on the future seismic design of bridges in Tennessee. USGS will use it to update the current seismic hazard maps used by TDOT engineers for the seismic design of bridges in Tennessee. This research will help TDOT engineers design future bridges that will be safer, save lives, and have a significant cost saving in the case of a seismic event.

Long-Term Implementation:

While this study does not provide TDOT engineers with that which can be immediately implemented, it provides a significant impact on updating seismic hazard maps that will be developed by the United States Geological Survey (USGS). American Associate of State Highway Transportation Officials (AASHTO) will use seismic hazard maps for the future seismic design specifications and, in turn, will be used by TDOT engineers to design bridges in Tennessee. In summary, this research will provide accurate and science-based results that will be used to improve seismic hazard maps employed for the seismic design of bridges in Tennessee.

Immediate Recommendations:

We recommend that the model provided in Supplement I: “A new model for vertical to horizontal response spectra for Central and Eastern North America” be used for developing the vertical response spectra for the design of bridges in Tennessee. Furthermore, the proposed model provided in Supplement II: “A ground-motion prediction model for small-to-moderate induced earthquakes for Central and Eastern United States,” could apply in long-term and short-term U.S. Geological Survey National Hazard maps for the hazard evaluation of induced seismicity in Tennessee. Finally, we propose using the model provided in Supplement III: “A ground-motion model for the Gulf Coast region of the United States,” be used for seismic design and assessment of bridges in West Tennessee.

Table of Contents

List of Tables

List of Figures

Glossary of Key Terms and Acronyms

AASHTO – American Associate of State Highway Transportation Officials (AASHTO)

CENA – Central and Eastern North America

GA – Genetic Algorithm

GMIM – Ground Motion Intensity Measures

GMMs – Ground Motion Models

HEM – Hybrid Empirical Method

NGA – Next Generation of Attenuation

M – Moment magnitude

PEER – Pacific Earthquake Engineering Research

USGS – United States Geological Survey

WNA – Western North America

Chapter 1 Introduction

The main objective of this study was to determine seismological parameters in Central and Eastern North America (CENA), including constraints on the geometrical spreading, anelastic attenuation, stress parameters, and site attenuation parameters (kappa). Details of the main objectives are provided in this report. In addition to the main objective, as part of this study, three new ground-motion models (GMMs) were developed: (1) a new model for vertical to horizontal response spectral ratios for central and eastern North America; (2) a ground-motion prediction model for small-to-moderate induced earthquakes for central and eastern United States; and (3) A Ground motion model for the Gulf Coast region of the United States, which includes part of West Tennessee. These three GMMs are presented as supplementary material to this report; and (3) A Ground motion model for the Gulf Coast region of the United States, which includes part of West Tennessee.

> *We used a genetic algorithm to invert weighted geometric mean estimates of horizontal response-spectral acceleration from the empirical NGA-East ground motion models... Also, as part of this study, we developed (1) A ground-motion prediction model for small-to-moderate induced earthquakes for Central and Eastern United States; (2) A New Model for Vertical to Horizontal Response Spectral Ratios for Central and Eastern North America; and (3) A Ground-Motion Model for the Gulf Coast Region.*

The stochastic point-source model (Boore, 2003) is one of the methods used to simulate earthquake ground motion intensity measures (GMIMs) in regions where recorded strong ground motions are sparse. Moreover, the stochastic method is used in the hybrid empirical method (HEM), introduced by Campbell (2003), to map empirical estimates of ground motion in a region with abundant strong ground motion data (host region) to a region that lacks such data (target region). For this purpose, the empirical estimation of ground motions for the host region is scaled by the ratio of stochastic simulations for the target region to those for the host region. The HEM approach has been used to develop GMMs for Central and Eastern North America (CENA) using the empirical ground-motion prediction equations for Western North America (WNA) (Tavakoli and Pezeshk, 2005; Pezeshk *et al*., 2011; Pezeshk *et al*., 2015, 2018). Because of the large ground-motion database in WNA, the seismological model parameters used for the host region are well-constrained. The inversion approach proposed in this study has been validated by Zandieh *et al*. (2016, 2018) using ground motions estimated from the NGA-West2 GMMs. Although that inversion was done on empirically simulated data from the NGA-West2 (GMMs), it demonstrates that the inversion methodology is feasible and results in seismologically realistic stochastic model parameters. This study is intended to improve our existing HEM-based GMM with the best seismological data and parameters for CENA by inverting the NGA-East ground-motion data used to implement GMMs for CENA. This is accomplished using the same methodology that was used to invert the simulated NGA-West2 GMM data to derive a consistent

set of seismological parameters for CENA that can be used in a stochastic model for this region as it is applicable to West Tennessee.

Chapter 2 Literature Review

For seismic hazard applications, ground-motion amplitudes are often estimated using GMMs. GMMs relate ground-motion intensity measures (GMIMs), such as peak ground acceleration (PGA), peak ground velocity (PGV), and 5%-damped pseudo-acceleration linear-elastic response-spectral acceleration (PSA) to seismological parameters in a specified region, such as earthquake magnitude, source-to-site distance, local site conditions, and style-of-faulting. In areas of the world where ground-motion recordings are plentiful due to their active seismicity and tectonics and there is a dense instrumental recording network [e.g., Western North America (WNA)], the GMMs are empirically obtained from a statistical regression of the ground-motion recordings (Douglas, 2003, 2011). An example of such empirical GMMs is those developed as part of the recent Pacific Earthquake Engineering Research (PEER) Next Generation Attenuation Phase 2 (NGA-West2) project (Bozorgnia *et al.*, 2014). Five individual GMMs were developed for WNA and other active tectonic regions in the world as part of the NGA-West2 project (Abrahamson *et al.*, 2014; Boore *et al.*, 2014; Campbell and Bozorgnia, 2014; Chiou and Youngs, 2014; Idriss, 2014). The inversion methodology used in this study has been used successfully to invert NGA-West2 GMMs for a consistent set of point-source seismological parameters that can be used in a stochastic simulation model for WNA (Zandieh *et al.*, 2018).

Empirical methods alone cannot be used to develop GMMs that are valid for moderate-to-large magnitudes for regions with limited strong ground-motion data. CENA (and West Tennessee) is an example of such a region, which is considered to be a stable continental region with abundant recordings of ground motion from mainly distant small and moderate-magnitude events but with limited ground-motion recordings from large-magnitude earthquakes of greatest engineering interest. In areas such as CENA, stochastic methods (e.g., Boore, 2003) are valuable and are often used to estimate ground motions for the distance and magnitude range of engineering interest (PEER, 2015). Stochastic ground-motion simulations are used to develop GMMs using the same empirical regression approach that is applied to recorded ground-motion data. In the simplest application of the stochastic simulation approach, a stochastic point-source method is used as a framework to estimate ground-motion time series and related GMIMs using simple seismological models of the source spectrum (Brune 1970, 1971), wave-propagation path, and local site conditions (McGuire and Hanks, 1980; Hanks and McGuire, 1981; Boore 1983, 2003, 2005). Atkinson and Boore (1995, 1998), Frankel *et al.* (1996), Toro *et al.* (1997), Silva *et al*. (2002), Campbell (2003, 2011), Pezeshk *et al.* (2011, 2015, 2108), and PEER (2015) are examples of GMMs that have been developed for CENA using the point-source stochastic method.

The HEM approach is also a well-accepted alternative procedure for developing GMMs in areas with limited ground-motion recordings. In the HEM approach, GMIMs in a target region (e.g., CENA) are predicted from empirical GMMs in a host region (e.g., WNA) using seismological-based adjustment factors between the two regions. The adjustment factors are calculated as the ratio of stochastically simulated GMIMs in the two regions. Using appropriate regional seismological parameters in the stochastic simulations, the calculated adjustment factors take into account differences in earthquake source, wave propagation, and site-response characteristics between the two regions. The empirically derived GMMs for the host region are transferred to the target region by applying the regional adjustment factors to the empirical GMIM predictions, from which a GMM is derived using standard regression analysis. The HEM

approach has been used by several researchers to develop GMMs in CENA (Campbell, 2003, 2007, 2008, 2011; Tavakoli and Pezeshk, 2005; Pezeshk *et al.*, 2011, 2015, 2018) in central Europe (Scherbaum *et al.*, 2005), and in southern Spain and southern Norway (Douglas *et al.*, 2006). Another method that is a well-accepted procedure for developing GMMs is the referenced empirical approach introduced by Atkinson (2008). It is similar to the HEM approach, but adjustment factors are calculated empirically using spectral ratios of observed motions in the target region to predictions of empirical GMMs in the host region (Atkinson, 2008; Hassani and Atkinson, 2014) and is, therefore, restricted only to the range of magnitude and distances that represent the recordings.

All of the stochastic models in CENA that have been used to date to develop GMMs either directly from simulations or indirectly using the HEM approach have used seismological parameters developed from recordings. Several of these studies have used broadband inversion of Fourier amplitude spectra, similar to, but not identical to, the method used in this study (e.g., Toro *et al.*, 1997; Silva *et al.*, 2002). To the best knowledge of the author, this study would be the first to perform a formal inversion using the extensive and peer-reviewed CENA GMMs developed for the NGA-East project (PEER, 2015; Goulet *et al.* , 2018) and using a formal genetic algorithm (GA) approach. The approach has been validated by using simulated small-to-moderate magnitude and large-magnitude data derived from the NGA-West2 GMMs (Zandieh *et al*., 2016, 2018).

Seismological parameters obtained in this research can be used to develop a new HEM ground motion model from the set of inverted seismological parameters to update that of Pezeshk *et al*. (2018). This will be a significant improvement because we used a set of consistent and well-correlated seismological parameters inverted from recorded data. Developing an updated GMM for CENA constitutes the future phase of this project.

Chapter 3 Methodology

Scherbaum *et al.* (2006) used a GA to determine seismological parameters for sets of stochastic models that matched empirically derived GMMs. Zandieh *et al.* (2018) were successfully able to perform a similar GA approach using NGA-West2 GMMs to determine seismological parameters for WNA. In this study, a GA is used to perform a point-source inversion for events and sites with R_{RUP} ≤ 300 km, moment magnitude (**M**) 4 to 8, and V_{S30} = 3,000 m/sec. The distance cutoff restricts the recordings to those that can be expected to be completely triggered and, therefore, provide an unbiased representation of the median ground motion. The derived model parameters can be used to support further stochastic and HEM applications to derive GMMs for CENA. Pezeshk *et al.* (2015) used the existing seismological parameters for CENA in their HEM model but, because CENA seismological parameters were adopted based on parameters derived from various studies, the authors had to use a calibration factor to match the observed data and there was no guarantee that the parameters were appropriately correlated. This calibration factor may be significantly reduced or even eliminated if we use a single consistent set of actual inverted seismological parameters, which maintains their strong inter-correlation. Table I provides a list of some of the seismological parameters needed to perform point-source stochastic analysis.

The goal of this study is to find the set of seismological parameters to use with a simple stochastic model that minimizes the misfit between the stochastically predicted values with the observed values. Both predicted and observed values are compared for the reference rock, which will be discussed later. The misfit between the stochastic model and the recordings (observations) is defined by the following residuals:

$$res_{i,j,k} = \left(\log(S_{i,j,k}) - \log(G_{i,j,k})\right)^2 \quad (1)$$

where $S_{i,j,k}$ is the observed value of the GMIM for magnitude i, distance j, and spectral period k, and $G_{i,j,k}$ is the stochastically predicted value of the GMIM for magnitude i, distance j, and spectral period k.

In this study, a GA is used to find the best combination of seismological parameters for use with a stochastic model similar to the methodology proposed by Holland (1975) and Goldberg (1989). It provides a formal mathematical framework for deriving a set of inter-correlated parameters for a specified model. The GA focuses on a population of variables, which are created randomly in the range defined by the physical constraints imposed by the model. Variables are grouped into sets; each of which is called a string and composed of a series of characters that defines a possible solution to the problem. The performance of the variables, as described by the objective function and the set of constraints, is represented by the fitness of each string. A mathematical expression, called a fitness function, calculates a value for a solution of the objective function. The best-fit solution gets the higher value, and the ones that violate the objective function and constraints are penalized. Therefore, like what happens in nature, the best-fit solutions survive (i.e., akin to Darwin's "survival of the fittest") and get the chance to be a parent of the next generation of parameter solutions. In a crossover procedure, two selected

parents reproduce the next generation. The procedure first divides the selected parent strings into segments and then some of the segments of the parent string are exchanged with corresponding segments from another parent string. Like in nature, this "mutation" guarantees diversity in the generated populations. This is done by flipping a randomly selected bit (i.e., 0 to 1 or vice-versa) in the selected binary string to create a mutated string. The mutation prevents a fixed model of solutions from being transferred to the next generation (Holland, 1975; Goldberg, 1989).

TABLE I
MEDIAN SEISMOLOGICAL PARAMETERS FOR CENA. (VALUES HIGHLIGHTED IN RED ARE TO BE DETERMINED FROM THE DATA BY GA INVERSION.)

Parameter	CENA
Source spectrum	**Single corner frequency** ω^2
Stress parameter, $\Delta\sigma$ **(bars)**	**From inversion**
Source velocity, β_s **(km/sec)**	**Boore (2016)**
Source density, ρ_s **(gm/cc)**	**Boore (2016)**
Geometric spreading	$$Z(R)=\begin{cases} R^{b1} & R \le R_1 \\ R_1^{b1}\left(\frac{R}{R_1}\right)^{b2} & R_1 < R \le R_2 \\ R_1^{b1}\left(\frac{R_2}{R_1}\right)^{b2}\left(\frac{R}{R_2}\right)^{b3} & R > R_2 \end{cases}$$ ***R_1*=50 km and *R_2*=125 km** **Coefficients *b_1*, *b_2*, and *b_3* will be determined from inversion.**
Quality factor, *Q(f)*	**From inversion**
Source duration, T_s **(sec)**	***$1/f_0$***
Path duration, T_p **(sec)**	**Boore and Thompson (2015)**
Site amplification, $A\ f$	**Hashash *et al.* (2020) and Stewart *et al.* (2020).**
Site attenuation, *K_0* (sec)	**From inversion**
Effective-depth parameter, *h* (km)	**From inversion**

The GA tries different combinations of the variables and finds the best solution, which minimizes the sum of the residuals defined in Equation (1) over all magnitudes, distances, and spectral periods of interest. Therefore, the objective function that is minimized by the GA is defined as:

$$Objective\ Function = \sum_{i,j,k} res_{i,j,k} \quad (2)$$

In this study, the inversion of the CENA data was performed using the median of the NGA-East GMMs (Goulet *et al.,* 2015). As noted before, a point-source inversion is performed for events and sites with $R_{RUP} \leq 300$ km. The CENA reference hard-rock site condition recommended by Hashash *et al.* (2014a) of V_{S30} = 3000 m/sec is adopted for this study. The ground-motion recordings to the CENA reference hard-rock condition using a methodology similar to that used in the published study by Hashash *et al.* (2020) and Stewart *et al.* (2020). These authors developed site amplification functions to adjust NGA-East recordings to the CENA reference rock condition. They developed linear and nonlinear amplification functions for response spectral accelerations and smoothed Fourier amplitude spectra. They developed models that are modular and can be used with and without the period or depth terms. If terms such as the site period or the sediment depth are available, they will be used which will improve the model estimation.

3.1 Stochastic Ground-Motion Simulation

Pezeshk *et al.* (2018) developed a set of computer routines based on the random vibration method of Kottke and Rathje (2008) to perform the point-source stochastic simulation of GMIM amplitudes using a seismological model. These computer routines have been checked and used in the development of an NGA-East GMM based on the HEM approach (Pezeshk *et al.*, 2015). In the stochastic method, the ground-motion acceleration is modeled as filtered Gaussian white noise modulated by a deterministic envelope function defined by a specified set of seismological parameters (Boore, 2003). The filter parameters are determined by either matching the properties of an empirically defined spectrum of strong ground motion with theoretical spectral shapes or using reliable physical characteristics of the earthquake source and propagation media (Hanks and McGuire, 1981; Boore, 1983, 2003). Additionally, Atkinson *et al.* (2009) and Boore (2009) investigated the relationship between the stochastic point-source model, SMSIM, (Boore, 2005) and the stochastic finite-fault model, EXSIM, (Motazedian and Atkinson, 2005) and suggested how the two could be aligned to give better agreement in predicted motions from small earthquakes at large distances, where the two models should provide similar results. In other words, both the point-source and finite-fault stochastic simulation methods give similar results for small earthquakes that can be represented by a point source, which is the assumption used in this study. However, as successfully demonstrated by Pezeshk *et al.* (2018), there are simple ways of including finite-source effects in the extrapolation of the point-source model to large earthquakes.

In the point-source model, the total Fourier amplitude spectrum (FAS) of the horizontal vibratory ground displacement, $Y(M_0,R,f)$, due to shear-wave propagation, can be modeled by the equation (Boore, 2003):

$$Y(M_0,R,f) = S(M_0,f)P(R,f)G(f)I(f) \quad (3)$$

where M_0 is the seismic moment (dyne-cm), R is the source-to-site distance (km), f is the frequency (Hz), $S(M_0, f)$ is the source spectrum, $P(R,f)$ is the path attenuation term, $G(f)$ is the site-response term, and $I(f)$ is a filter representing the type of GMIM. The FAS of acceleration is obtained by multiplying $Y(M_0, R, f)$ by omega-square, ω^2.

3.2 Effective Point-Source Distance

In the stochastic point-source model, the earthquake source is assumed to be concentrated at a point within the crust, which is a reasonable assumption for small earthquakes or when the source-to-site distance is considerably larger than the earthquake source dimensions. Otherwise, finite-fault effects in the form of magnitude and distance saturation begin to influence the ground motions.

Atkinson and Silva (2000) defined an effective point-source distance metric to use in point-source stochastic simulations to mimic the ground-motion saturation effects of a finite-fault model. They also defined a magnitude-dependent equivalent point-source depth, *h*, to modify this distance for magnitude-saturation effects. Following these authors, we define an effective point-source distance metric to use with our point-source stochastic simulations as given by the expression:

$$R_{PS} = \sqrt{R_{RUP}^2 + h^2} \tag{4}$$

where the pseudo-depth parameter, *h*, which is also referred to as the finite-fault factor by Boore and Thompson (2014). Pezeshk et al. (2018) used the following equation to determine the effective-depth parameter *h*:

$$\log h = \begin{cases} \max(-0.05 + 0.15\mathbf{M}, -1.72 + 0.43\mathbf{M}) & \mathbf{M} \le 6.75 \\ -0.405 + 0.235\mathbf{M} & \mathbf{M} > 6.75 \end{cases} \tag{5}$$

In this study, we determined the effective-depth, *h.* The effective point-source distance metric is used in stochastic simulations to mimic magnitude and distance saturation effects so that the stochastic simulations can be extrapolated beyond the small-to-moderate magnitudes that are being evaluated in this study.

3.3 Site Response

The site-response term *G*(*f*) is defined as the product of crustal amplification and diminution functions (Boore, 2003). Crustal amplification is calculated using the quarter-wavelength (QWL) method, which Boore (2013) refers to as the square-root-impedance (SRI) method. Boore (2003) proposes the maximum-frequency filter, f_{max} (Hanks, 1982), and the kappa filter, κ_0 (Anderson and Hough, 1984), as alternative methods of modeling the site diminution function. The preferred kappa filter, $\exp(-\pi\kappa_0 f)$, can be considered as the path-independent loss of energy in the ground motion as it propagates through the site profile. It is defined by Anderson and Hough (1984) as the high-frequency slope of the FAS on a log-linear plot, assuming an Omega-square Brune acceleration source spectrum. Although kappa can be calculated from a recording at any distance, the part of kappa that is associated with the crustal profile beneath the site, κ_0, includes attenuation from both wave scattering and material damping (e.g.,

Campbell, 2009) and can be calculated in a variety of ways depending on the size of the earthquake and the available recordings (Ktenidou *et al.*, 2014). In this study, the parameter κ_0 is used to define the site attenuation because of its common use in engineering seismology (Campbell, 2009; Ktenidou *et al.*, 2014). The parameter κ_0 is obtained from the inversion.

3.4 Site Characterization in CENA

Campbell (2003) and Tavakoli and Pezeshk (2005) used a CENA reference hard-rock site condition with a time-averaged shear-wave velocity in the top 30m of the site profile of V_{S30} ≈ 2800m/sec and a site attenuation of k_0 = 0.006 sec. They used the generic CENA hard-rock crustal-amplification model developed by Boore and Joyner (1997) in their stochastic models. Atkinson and Boore (2006), Pezeshk *et al.* (2011), and Campbell (2008, 2011) used an empirically derived CENA hard-rock crustal-amplification model corresponding to V_{S30} ≥ 2000 m/sec and κ_0 = 0.005 sec (Atkinson and Boore, 2006). In this study, CENA reference hard-rock site condition recommended by Hashash *et al.* (2014a) for use in the NGA-East project that corresponds to V_{S30} = 3000 m/sec has been adopted. We invert for k_0 along with other seismological parameters to make sure that k_0 is well correlated and consistent with the other parameters. For the point-source stochastic model, we used a crustal amplification model for the CENA reference hard-rock condition after a thorough literature review. The crustal amplification factors derived by Boore and Thompson (2015), based on the QWL method and the velocity profile of Boore and Joyner (1997) modified to have a shear-wave velocity of 3,000 m/sec over the top 300 m, was used to adjust NGA-East recordings in Boore (2015) and Boore and Campbell (2017).

As discussed before, to adjust the NGA-East ground motions to the CENA reference hard-rock condition, we used the Hashash *et al.* (2020) and Stewart *et al.* (2020) models.

3.5 Source Model

The Brune (1970, 1971) ω^2-source spectrum was used in the stochastic simulations. Brune's model is a single-corner frequency (f_0) point-source spectrum in which the stress parameter ($\Delta\sigma$) controls the spectral shape at high frequencies.

3.6 Stress Parameter in CENA

Boore *et al.* (2010) used the point-source stochastic simulation program SMSIM (Boore, 2005) to determine the stress parameters for eight well-recorded earthquakes in CENA. They showed that estimates of the stress parameter, $\Delta\sigma$, are strongly correlated to the rate of geometrical spreading in the near-source region. Using the geometrical spreading and quality factor (Q) relationships from Atkinson (2004), hereafter referred to as A04, they estimated a geometric mean value of $\Delta\sigma$ = 250 bars for the case in which the 1988 Saguenay earthquake was included and 180 bars for the case in which the Saguenay event was excluded. Atkinson *et al.* (2009) and Boore (2009) also found, after adjusting other parameters in the model, that a stress parameter of 250 bars instead of 140 bars was needed to bring the stochastic point-source results of SMSIM in line with the stochastic finite-fault results of EXSIM (Motazedian and Atkinson, 2005) used in Atkinson and Boore (2006), for small distant earthquakes. Campbell (2008, 2011)

had initially estimated this point-source stress parameter as $\Delta\sigma$ = 280 bars. Atkinson and Assatourians (2010) analyzed recordings of the **M** 5.0 Val-des-Bois, Quebec earthquake using the A04 attenuation model and also found a stress parameter of 250 bars.

In their revision of the CENA seismological model, Boore and Thompson (2015) found that a stress parameter of 400 bars was needed to approximate the amplitude of the ground motions that matched the A04 attenuation term and the Atkinson and Boore (1995) path duration term when the new energy-based significant duration parameter recommended by Boore and Thompson (2014) was used. The higher value of $\Delta\sigma$ was needed to compensate for the smaller amplitudes predicted from the stochastic ground-motion simulations when the longer path durations predicted by the new duration model were used, which spreads the radiated energy from the point source over a longer duration. In this study, the stress parameter is obtained from the GA inversion. The inverted stress parameter is properly correlated with the adopted path attenuation and path duration and the other seismological parameters that are either constrained or determined from the GA inversion.

3.7 Source and Path Duration

The sum of the source duration (T_S) and the path duration (T_P) represents the total duration of ground motion in the stochastic method. The source duration for the Brune single-corner frequency model is typically defined (e.g., Boore, 2003) as the inverse of the source corner frequency, $1/f_0$. Boore and Thompson (2015), using the NGA-East database (Goulet *et al.*, 2014), derived a distance-dependent T_P relationship for stable crustal regions, such as CENA.

Up until now, the terms in the seismological model have been defined in terms of Fourier Amplitude Spectrum (FAS), whereas the NGA-EAST GMMs predict 5%-damped pseudo-absolute acceleration response spectra (PSA). To invert the predicted values of PSA for a set of seismological parameters defined in terms of FAS, we must have a means of converting between the two types of GMIMs. This is done with the GMIM response term $I(f)$ in Equation (3). This term can be evaluated either in the time domain using simulation or in the frequency domain using random vibration theory (RVT). In this study, we use the RVT approach built into the point-source stochastic simulation program STRATA (Kottke and Rathje, 2008).

The RVT method requires an estimate of the total response duration of the GMIM of interest (Boore, 2003). This is calculated as the sum of the source duration T_S and the path duration T_P. The path-duration terms proposed by Boore and Thompson (2015) are used in this study, which is provided in Table II for completeness since it is not possible to derive a path-duration model from the inversion due to the large number of parameters involved. We emphasize that the adopted path duration model is based on the recent NGA-East database and is, therefore, consistent with the data we are using in this study.

We used their new path-duration term because of its consistency with the database used to develop the NGA-EAST GMMs. Boore and Thompson (2014) defined the distance-dependence of the path duration in terms of R_{RUP}, but Boore and Thompson (2015) noted that it should be defined in terms of R_{PS} to be consistent with the use of this latter distance metric in the stochastic simulations. The resulting path durations are given in Table II. They are constrained in the inversions because of their strong correlation with other seismological parameters in the model.

TABLE II
PATH DURATION MODELS (BOORE AND THOMPSON 2015)

R_{PS} (km)	T_P (sec)
0	0.0
15	2.6
35	17.5
50	25.1
125	25.1
200	28.5
392	46.0
600	69.1
Slope of last segment	0.111

3.8 Path Attenuation

The path term $P(R,f)$ in Equation (3) is separated into two components, commonly referred to as geometrical attenuation (or spreading), $Z(R)$, and anelastic attenuation, $Q(f)$. Geometrical attenuation models the amplitude decay due to the expanding surface area of the wave front as it propagates away from the source. Anelastic attenuation, quantified by the quality factor Q, models the amplitude decay due to the conversion of elastic wave energy to heat and wave scattering and is usually found to be frequency-dependent. Boore *et al.* (2010) found that the stress parameter is strongly correlated to the choice of geometrical spreading, which reiterates the fact that the set of seismological parameters for a given region must be internally consistent and should not be taken from different studies with vastly different assumptions, which is one of the strengths of this study. The path-attenuation parameters for CENA that are derived from the GA inversion are presented in the following sections.

3.8.1 Path Attenuation for CENA

Boore *et al*. (2010) used four geometrical attenuation models ranging from a simple R^{-1} decay for all distances to more complicated bilinear and trilinear distance decay models to determine the stress parameter for eight well-recorded earthquakes in CENA. Atkinson and Assatourians (2010) studied five well-recorded CENA earthquakes and found that the ground motions were better fit if the A04 geometrical attenuation model, with $R^{-1.3}$ near-source spreading, is used for hypocentral distances beyond 10 km and a $R^{-1.0}$ decay is used at shorter distances. Campbell (2007, 2008, 2011) and Pezeshk *et al.* (2011) used the original A04 path-attenuation model. Pezeshk *et al*. (2018) used the path attenuation model developed by Chapman *et al*. (2014). These authors used broadband recordings from the EarthScope Transportable (TA) Array and an iterative inversion process to derive a trilinear geometric attenuation model with $R^{-1.3}$ spreading to 60 km, R^{0} (no spreading) from 60 to 120 km, and $R^{-0.5}$ for L_g-wave spreading beyond 120 km.

In this study, the path-attenuation terms are obtained from the GA inversion. A trilinear geometrical attenuation term with transition distances of 50 km and 125 km will be used to perform the inversions. These transition distances are selected to match the CENA transition

distances used by Boore and Thompson (2015) in their path-duration model (Figure 3-1), since one would expect the two to be strongly correlated. We explored the use of other transition distances and even the possibility of a bilinear rather than a trilinear model if the data support them.

Following seismological convention, anelastic attenuation will be defined by the expression $Q(f) = Q_0 f^{\eta}$, where $Q(f)$ increases with frequency ($\eta \geq 0$). Assuming a trilinear model, the geometrical spreading function, $Z(R)$, is given by a piecewise equation defined as:

$$Z(R) = \begin{cases} R^{b1} & R \leq R_1 \\ R_1^{b1}\left(\frac{R}{R_1}\right)^{b2} & R_1 < R \leq R_2 \\ R_1^{b1}\left(\frac{R_2}{R_1}\right)^{b2}\left(\frac{R}{R_2}\right)^{b3} & R > R_2 \end{cases} \quad (6)$$

where the coeffcients b_1, b_2, and b_3 will be determined in the GA inversion. For the trilinear model, b_3 is associated with the decay of L_g waves at regional distances. The anelastic and geometrical attenuation functions obtained from the GA inversion and are compared with values obtained by Chapman *et al.* (2014), who derived Q_0 and η for CENA using 16 recorded events in this report.

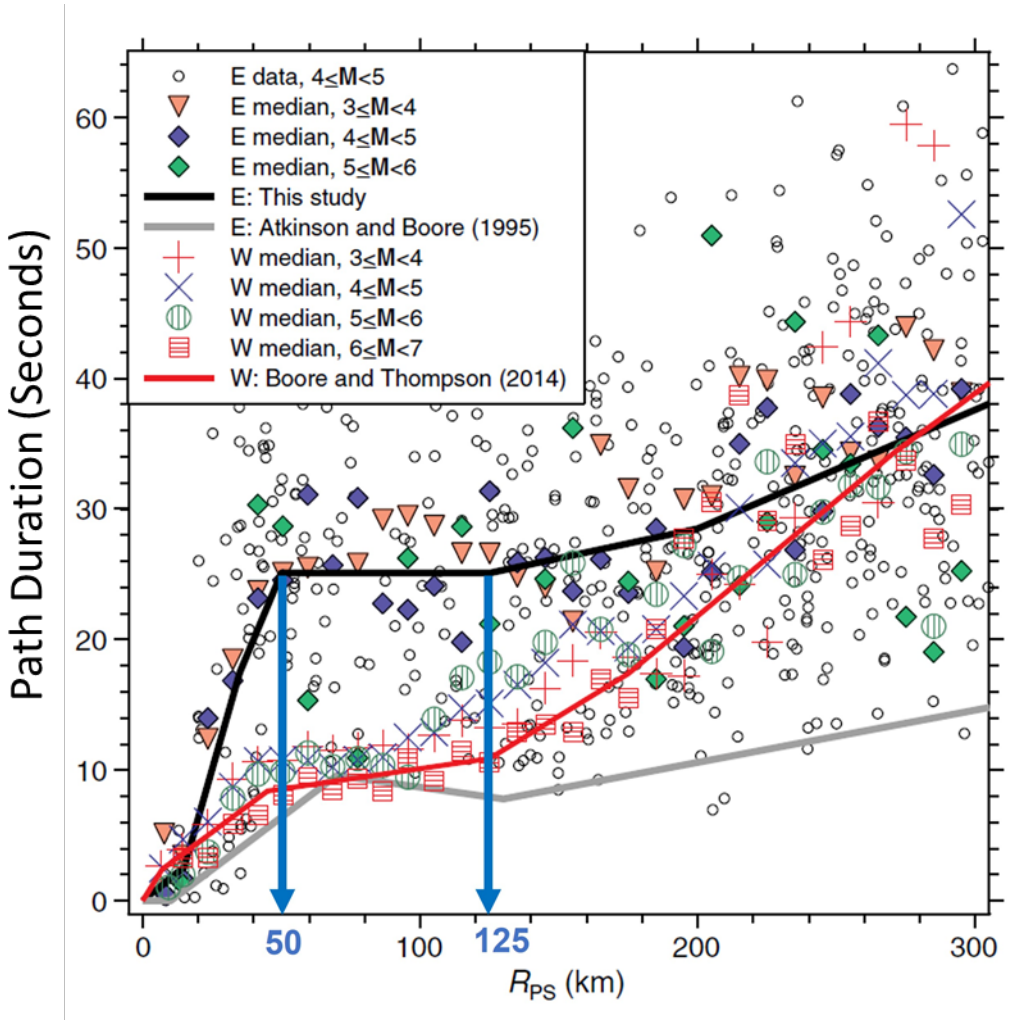

Figure 3-1. Path-duration models for CENA and WNA (modified from Boore and Thompson, 2015). In the legend, E represents Central and Eastern United States and W represents western North America. The x-axis represents the effective point-source distance metric, R_{PS}, and the y-axis represents the path duration D_P.

3.9 Genetic Algorithmic Inversion

Table I provided a list of the seismological models and parameters that are needed to perform the point-source stochastic simulation. Table I indicated which ones are obtained from the literature and which are derived in the GA inversion. As indicated in the previous section, the constrained models and parameters are taken from recently published research because they are either too complex or too strongly correlated with other parameters to allow the inversion to converge. The remaining parameters are derived from the inversion. We used a GA inversion to determine the best combination of the remaining seismological parameters for the point-source stochastic model that matches the weighted median GMIMs predicted from the five NGA-EAST GMMs.

As Table I indicated, the seismological parameters determined in the inversion are $\Delta\sigma$, b_1, b_2, b_3, Q_0, η (eta), and *h.* Constraints are imposed on these parameters to keep them within reasonable limits in the inversion (Table III). All other parameters are held constant in the inversion. The inversion is performed for individual **M** ranging from 4.0 to 8.0 in 0.5 intervals (10 magnitudes), at 25 periods ranging from 0.01 to 10 sec, uniformly distributed in log-space, and at 30 values of R_{RUP} ranging from 1 to 300 km, uniformly distributed in log-space. Parameters are obtained for each magnitude. The parameter b_1 is obtained for each frequency used in the inversion.

TABLE III

CONSTRAINTS IMPOSED ON PARAMETERS IN THE GA INVERSION

Parameter	Search Range
b_1	-1.3 to -0.5
b_2	-1.2 to 0.5
b_3	-1.2 to 0.5
a**	-1.5 to -0.7
b**	0.1 to 0.5
$\Delta\sigma$	100 to 150
Q_0	300 to 550
η	0.4 to 0.7
κ	0.005 to 0.01

a and b are used to calculate the effective depth term, h(M**), using $\log_{10}(h(\mathbf{M})) = a + b\mathbf{M}$

Table IV provides the model parameters determined from the GA inversion. The geometrical spreading coefficient b_1 is shown in Figure 3-2. The geometrical spreading coefficients b_2 and b_3 are shown in Figure 3-3. All parameters were determined for each magnitude used in the inversion, except for b_1, which was determined differently for each magnitude and frequency used in the inversion. b_2 and b_3 did not vary with frequency to avoid a trade-off between coefficients. The near-source geometrical spreading coefficient, b_1, is both frequency-dependent and magnitude-dependent. As can be observed from Figure 3-2, there is a slight decrease of the b_1 for 0 Hz ≤ f ≤ 0.2 Hz frequency range for magnitudes **M** > 5.5, an increase for 0.2 Hz ≤ f ≤ 20 Hz frequency range, and almost no change for 20 Hz ≤ f ≤ 100 Hz frequency range. Overall, the b_1 paramters varies a minimum value of 1.127 for **M** 7 for f = 0.178 Hz to a maximum value of -0.27 for **M** 4 for f = 100 Hz. The coefficient b_2 varies from a minimum value of -0.745 to a maximum value of -0.409 for magnitudes, **M**, in the range of 4 to 8. The coefficient b_3 varies a minimum of from -0.549 to a maximum value of -0.402 for magnitudes, **M**, in the range of 4 to 8.

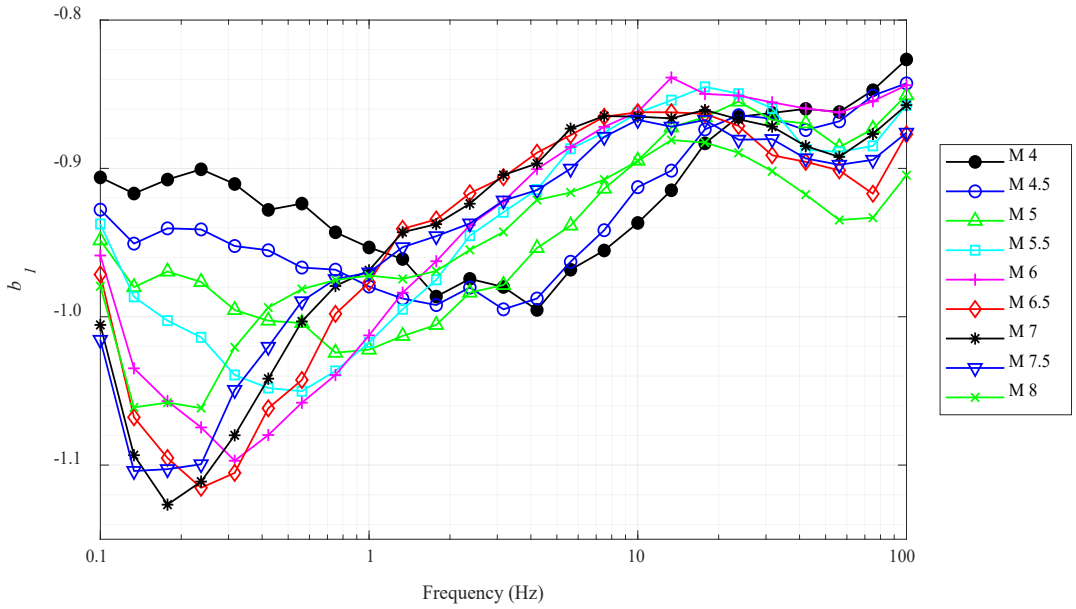

Figure 3-2. Geometrical spreading coefficients obtained from the genetic algorithm (GA) inversion of the Next Generation Attenuation-East (NGA-East) ground-motion models (GMMs): the coefficient b_1 is as a function of magnitude and frequency. The y-axis represents the parameter b_1.

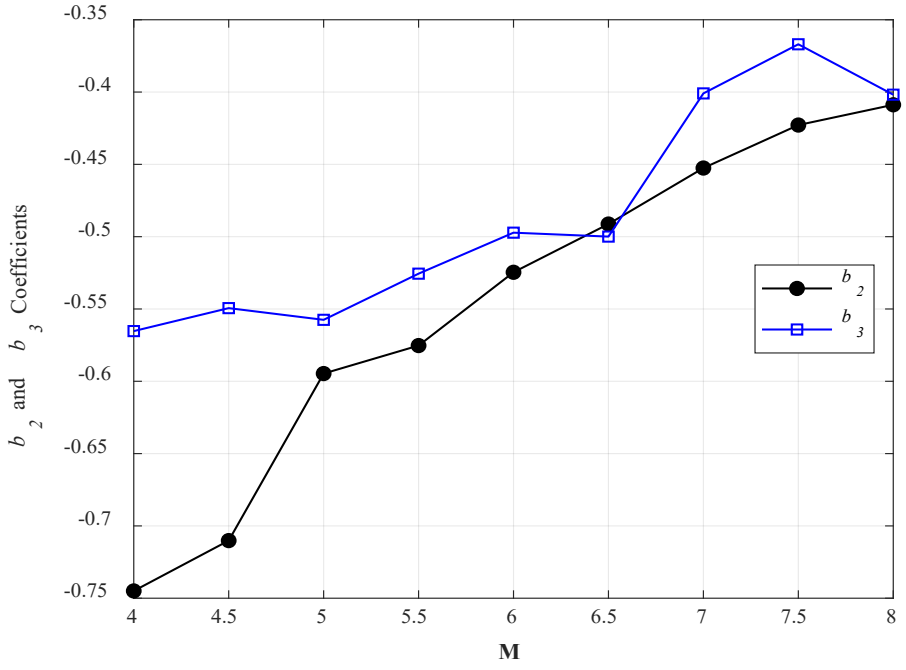

Figure 3-3. Geometrical spreading coefficients obtained from the genetic algorithm (GA) inversion of the Next Generation Attenuation-East (NGA-East) ground-motion models (GMMs): coefficients b_2 and b_3 are a function of magnitude. The y-axis represents the parameters b_2 and b_3.

Figure 3-4 shows the effective-depth term. The effective depth term obtained from inversion, h(M) increases from about 2.66 km to 17.66 km as the magnitude, **M,** increases from 4 to 8. An exponential model was fitted to the results given by: $\log_{10}(h) = -0.409 + 0.207\mathbf{M}$.

Figure 3-5 shows the stress parameter, $\Delta\sigma$ values obtained from the inversion. The stress parameter $\Delta\sigma$-value fluctuates between 104 bars to 117 bars for various magnitudes.

Figure 3-6 shows the anelastic attenuation parameters, Q_0 and η, and their corresponding quality factor function, $Q(f)$, for different magnitudes obtained from inversion. The parameter Q_0 varies from 430 to 500 and η varies from 0.573 to 0.649, resulting in a quality factor function that increases exponentially from 0 to a mean of 6000 as the magnitude, **M,** increases from 4 to 8.

Figure 3-7 shows the high-frequency Fourier amplitude spectrum (FAS) decay parameter κ (kappa) obtained from inversion. The attenuation parameter κ obtained from inversion varies from 0.0067 to 0.0091.

It is important to note that all seismological parameters that obtained from this study (stress parameter, kappa, geometrical spreading, and anelastic attenuation) are self-consistent and properly correlated, and based on the same recorded data. This is an advantage over existing stochastic models whose parameters have been obtained by various researchers from published work and, therefore, are not necessarily correlated. For example, Boore *et al.* (2010) showed that estimates of the stress parameter ($\Delta\sigma$) are strongly correlated to the rate of geometrical spreading in the near-source region.

The purpose of this study was to determine the seismological parameters for CENA. Updating of Pezeshk *et al.* (2018) will be part of a future project, and it is not part of this report. The same procedure used by Pezeshk *et al.* (2008) will be used for the proposed update using the seismological parameters obtained in this study.

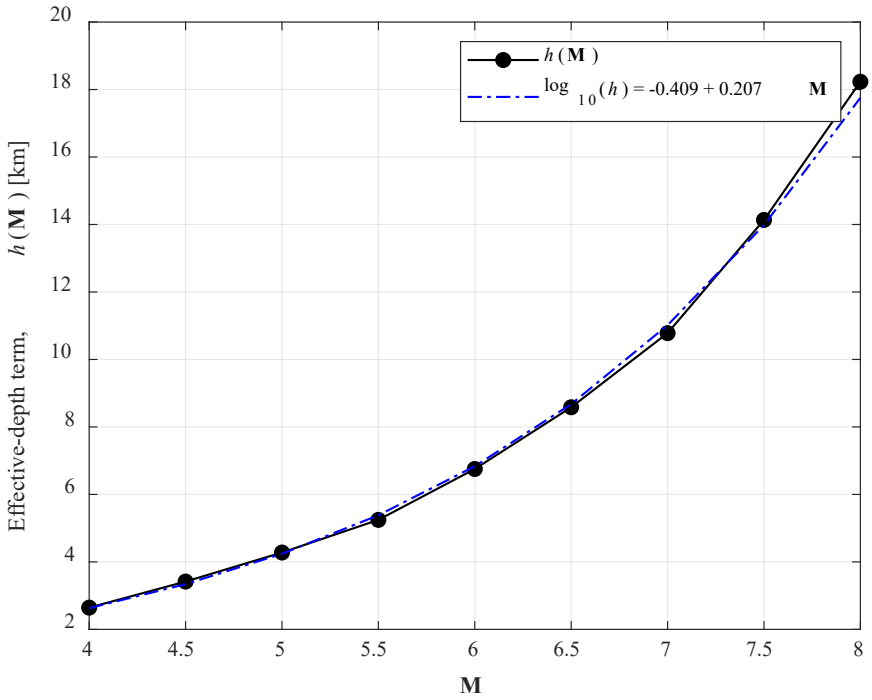

Figure 3-4. Effective-depth term h(M) obtained from the GA inversion of the NGA-East GMMs, along with the fitted functional form given by the equation $\log_{10}(h) = a + b\mathbf{M}$ (where a = -0.3994 and b = 0.1974, and r^2-value of 0.9972).

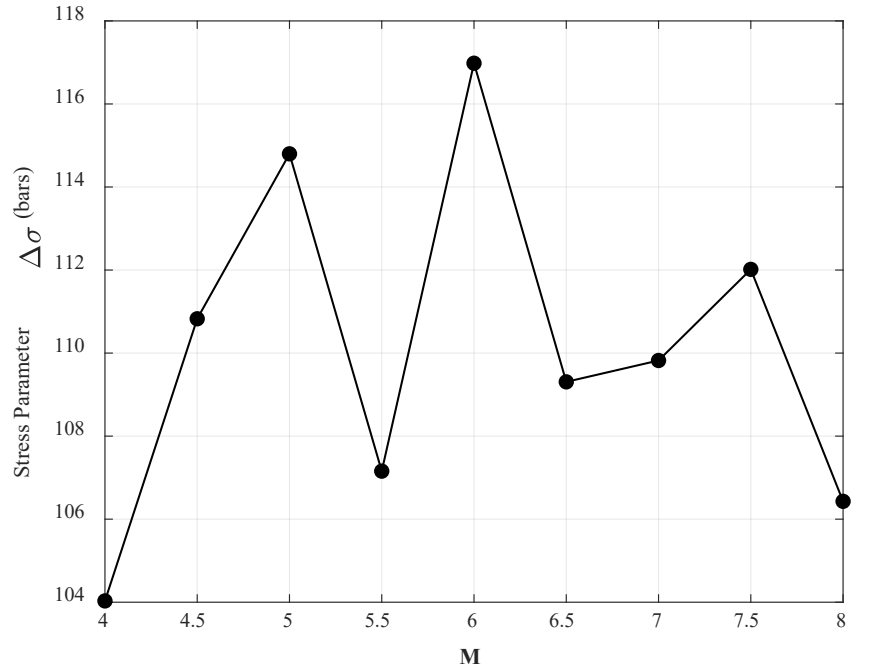

Figure 3-5. Stress Parameter $\Delta\sigma$-values obtained from GA inversion of the NGA-East GMMs as a function of magnitude.

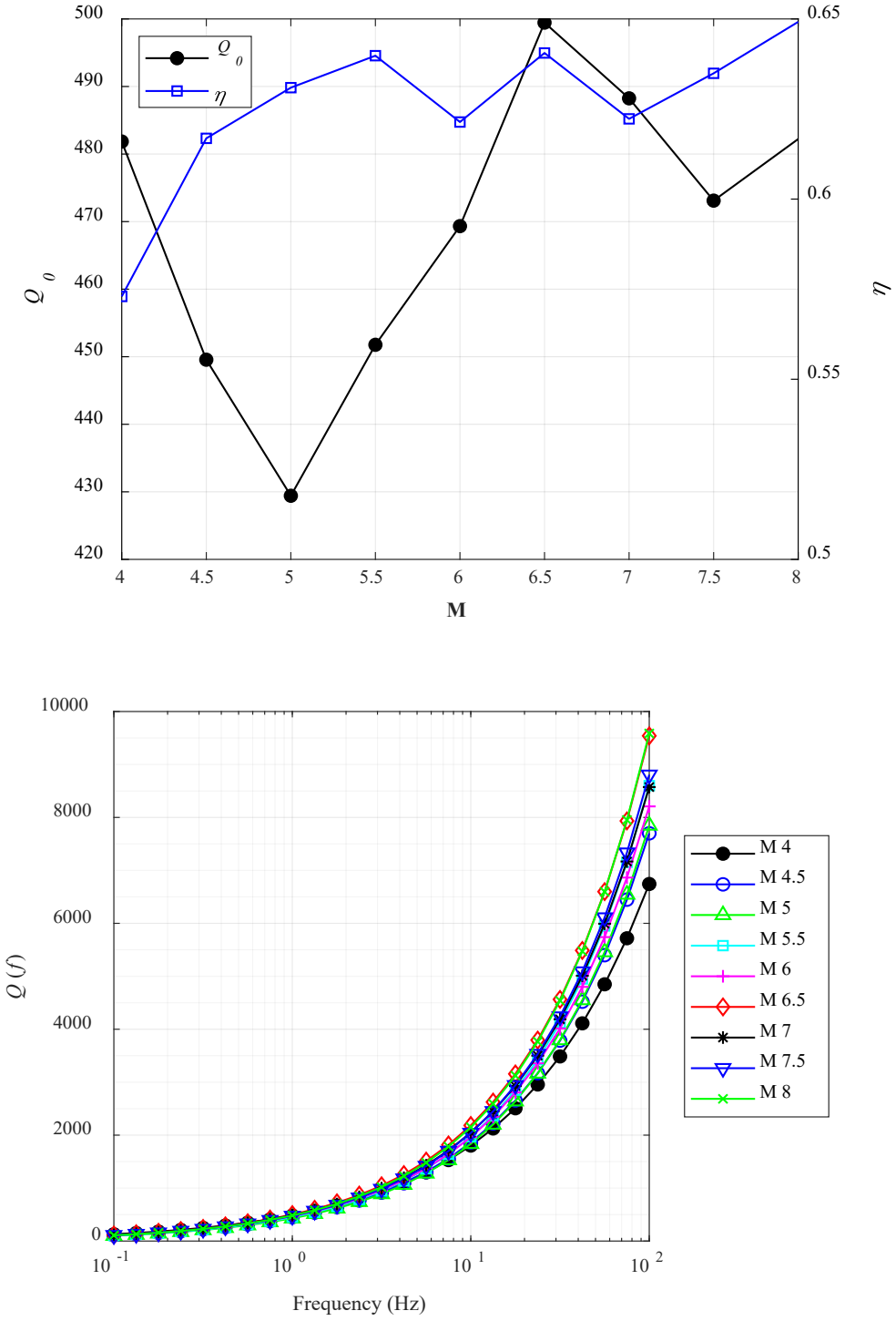

Figure 3-6. Anelastic attenuation parameters and model obtained from the GA inversion of the NGA-East GMMs: (Top Panel) Parameters Q_0 and η as a function of magnitude, (Bottom Panel) Quality factor function, $Q(f) = Q_0 f^{\eta}$ for different magnitudes as a function of frequency.

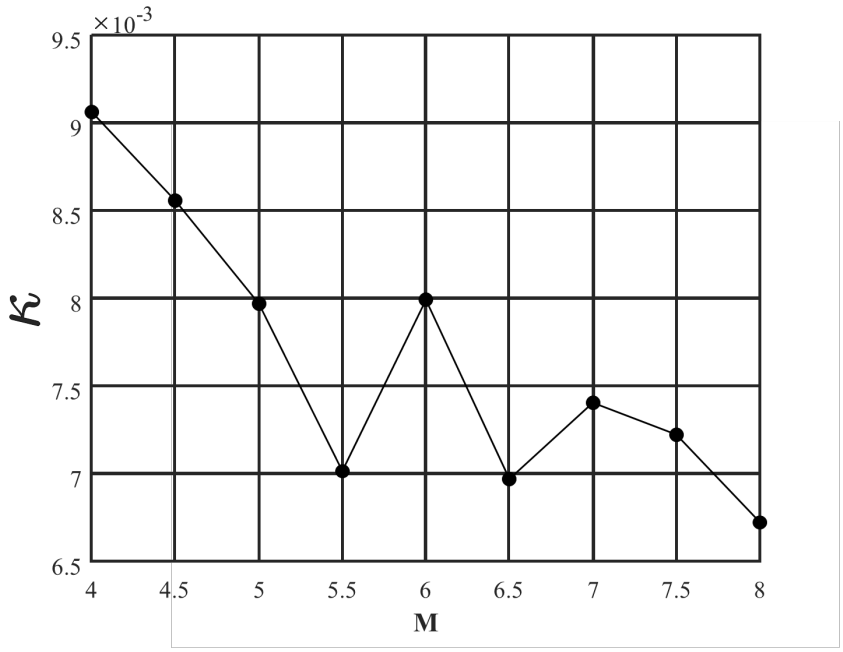

Figure 3-7. Shallow attenuation parameter κ (kappa) obtained from inversion of the NGA-East GMMs as a function of magnitude.

TABLE IV
COEFFEICIENT RESULTS OF THE GA INVERSION

M	$\Delta\sigma$	b_2	b_3	Q_0	η	κ	h
4	104.03	-0.745	-0.565	481.851	0.573	0.0091	2.65
4.5	110.83	-0.710	-0.549	449.557	0.617	0.0086	3.42
5	114.80	-0.595	-0.557	429.417	0.631	0.0080	4.28
5.5	107.16	-0.575	-0.526	451.764	0.640	0.0070	5.25
6	116.98	-0.525	-0.497	469.329	0.621	0.0080	6.75
6.5	109.31	-0.491	-0.500	499.453	0.641	0.0070	8.58
7	109.82	-0.453	-0.401	488.245	0.622	0.0074	10.78
7.5	112.02	-0.423	-0.367	473.104	0.635	0.0072	14.14
8	106.43	-0.409	-0.402	482.220	0.649	0.0067	18.23

TABLE IV – CONTINUED

b_1 (Hz)	0.100	0.133	0.178	0.237	0.316	0.442	0.562	0.750	1.000
M = 4	-0.906	-0.917	-0.908	-0.901	-0.911	-0.928	-0.924	-0.943	-0.953
M = 4.5	-0.928	-0.951	-0.940	-0.941	-0.952	-0.955	-0.967	-0.968	-0.980
M = 5	-0.948	-0.980	-0.970	-0.977	-0.995	-1.003	-1.004	-1.024	-1.022
M = 5.5	-0.937	-0.987	-1.003	-1.014	-1.039	-1.048	-1.050	-1.037	-1.017
M = 6	-0.959	-1.035	-1.057	-1.075	-1.097	-1.080	-1.058	-1.039	-1.013
M = 6.5	-0.972	-1.068	-1.095	-1.115	-1.105	-1.062	-1.043	-0.998	-0.977
M = 7	-1.006	-1.093	-1.127	-1.111	-1.080	-1.042	-1.003	-0.979	-0.969
M = 7.5	-1.016	-1.104	-1.103	-1.099	-1.049	-1.020	-0.990	-0.975	-0.970
M = 8	-0.979	-1.061	-1.058	-1.062	-1.021	-0.994	-0.981	-0.975	-0.972

b_1 (Hz)	1.334	1.778	2.371	3.162	4.217	5.623	7.499	10
M = 4	-0.961	-0.986	-0.974	-0.980	-0.995	-0.968	-0.955	-0.937
M = 4.5	-0.988	-0.992	-0.980	-0.995	-0.988	-0.963	-0.942	-0.913
M = 5	-1.013	-1.006	-0.984	-0.979	-0.954	-0.939	-0.914	-0.895
M = 5.5	-0.995	-0.975	-0.945	-0.930	-0.914	-0.887	-0.876	-0.863
M = 6	-0.984	-0.963	-0.938	-0.922	-0.900	-0.886	-0.872	-0.862
M = 6.5	-0.941	-0.934	-0.917	-0.906	-0.889	-0.878	-0.865	-0.862
M = 7	-0.943	-0.938	-0.924	-0.904	-0.897	-0.873	-0.865	-0.865
M = 7.5	-0.953	-0.946	-0.937	-0.922	-0.915	-0.900	-0.879	-0.867
M = 8	-0.975	-0.969	-0.955	-0.943	-0.921	-0.916	-0.908	-0.895

b_1 (Hz)	13.335	17.783	23.714	31.623	42.17	56.234	74.989	100
M = 4	-0.915	-0.883	-0.865	-0.863	-0.860	-0.862	-0.847	-0.827
M = 4.5	-0.902	-0.874	-0.864	-0.866	-0.874	-0.868	-0.851	-0.843
M = 5	-0.872	-0.865	-0.855	-0.867	-0.870	-0.886	-0.873	-0.851
M = 5.5	-0.854	-0.845	-0.850	-0.860	-0.887	-0.889	-0.885	-0.857
M = 6	-0.839	-0.850	-0.851	-0.855	-0.860	-0.862	-0.855	-0.844
M = 6.5	-0.862	-0.863	-0.871	-0.891	-0.896	-0.901	-0.917	-0.877
M = 7	-0.866	-0.861	-0.867	-0.872	-0.885	-0.892	-0.877	-0.857
M = 7.5	-0.872	-0.867	-0.881	-0.880	-0.893	-0.898	-0.894	-0.876
M = 8	-0.881	-0.883	-0.889	-0.902	-0.918	-0.935	-0.933	-0.905

Chapter 4 Results and Discussion

Figures 4-1 to 4-3 compare the median predicted response spectra from the NGA-EAST GMMs and the predicted response spectra from the inverted stochastic point-source model derived in this study. Results are shown for **M** = 4.0, 6.0 and 8.0 and R_{RUP} = 1, 5.872, 28.321, 62.198, 112.21, and 202.435 km. The standard deviation, $\sigma_{GMMS,Total}$, defined as:

$$\sigma_{GMMS,Total} = \sqrt{\sigma_{within-GMMS+}\ \sigma_{between-GMMS}} \quad (7)$$

where the parameter $\sigma_{within-GMMs}$ is the average within-model uncertainty in median predictions of the NGA-East models. $\sigma_{between-GMPEs}$ is between the NGA-east GMM predictions from GMMs. Figure 4-1 to Figure 4-3 compare the median response spectra of the NGA-East GMMs to the predicted response spectra from this study. Results are shown for **M** 4.0, 6.0, and 8.0, and R_{RUP} = 1, 5.872, 28.321, 62.198, 112.21, and 246.435 km. The highlighted area is the NGA-East GMM predictions ±σ, where σ represents $\sigma_{within-GMMs}$ estimated from the NGA-East report. Figure 4-1, Figure 4-2, and Figure 4-3 show good agreement between the median NGA-East GMMs and the inverted stochastic model. The predicted PSA values are well within one standard deviation of the median NGA-East GMM predictions.

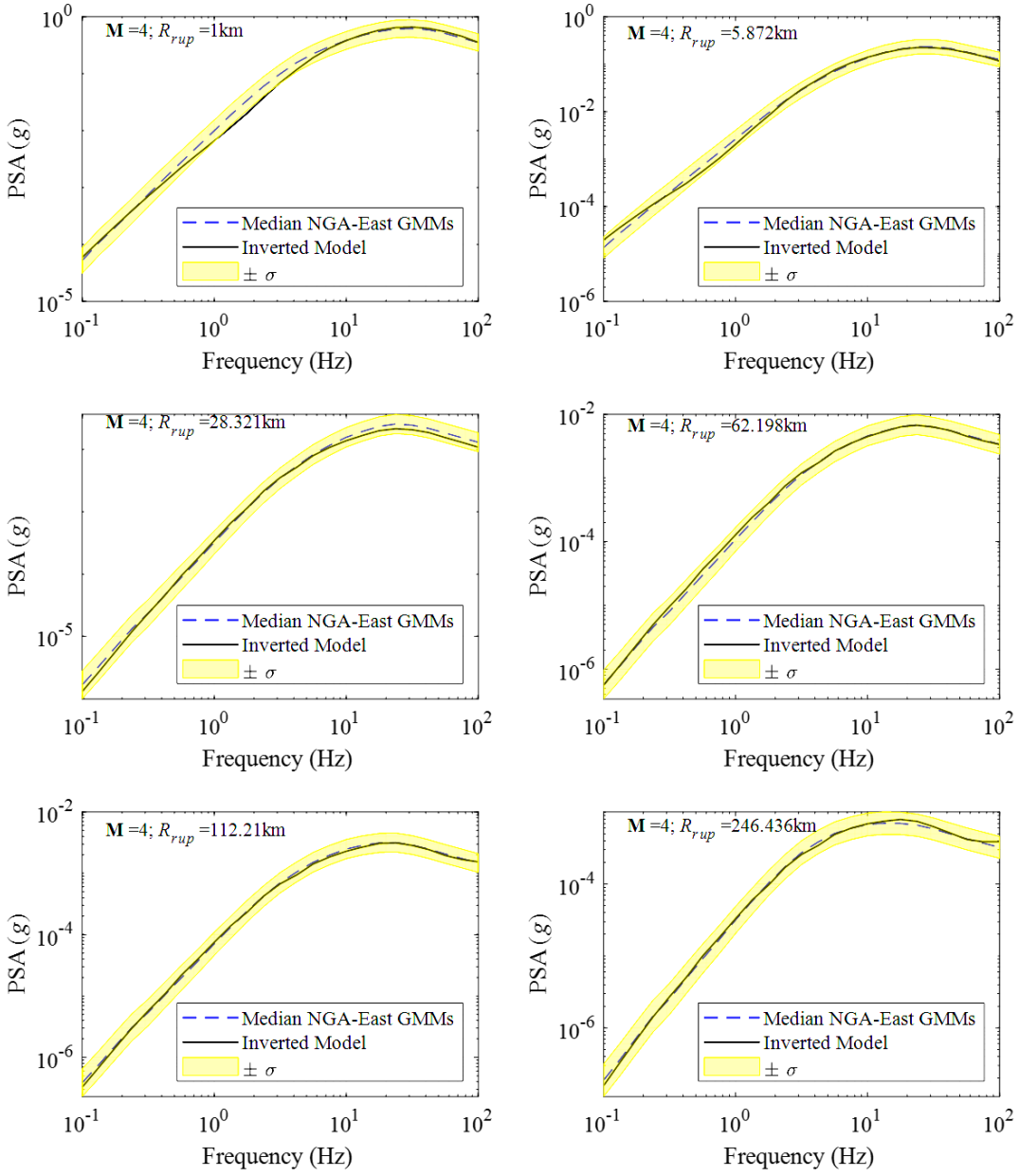

Figure 4-1. Comparison of the predicted response spectra from the median NGA-East GMMs with the predicted response spectra obtained from the model obtained from the GA inversion of the NGA-East GMMs for **M** 4. The highlighted area is the NGA-East GMM predictions ±σ, where σ is the standard deviation of the NGA-East model.

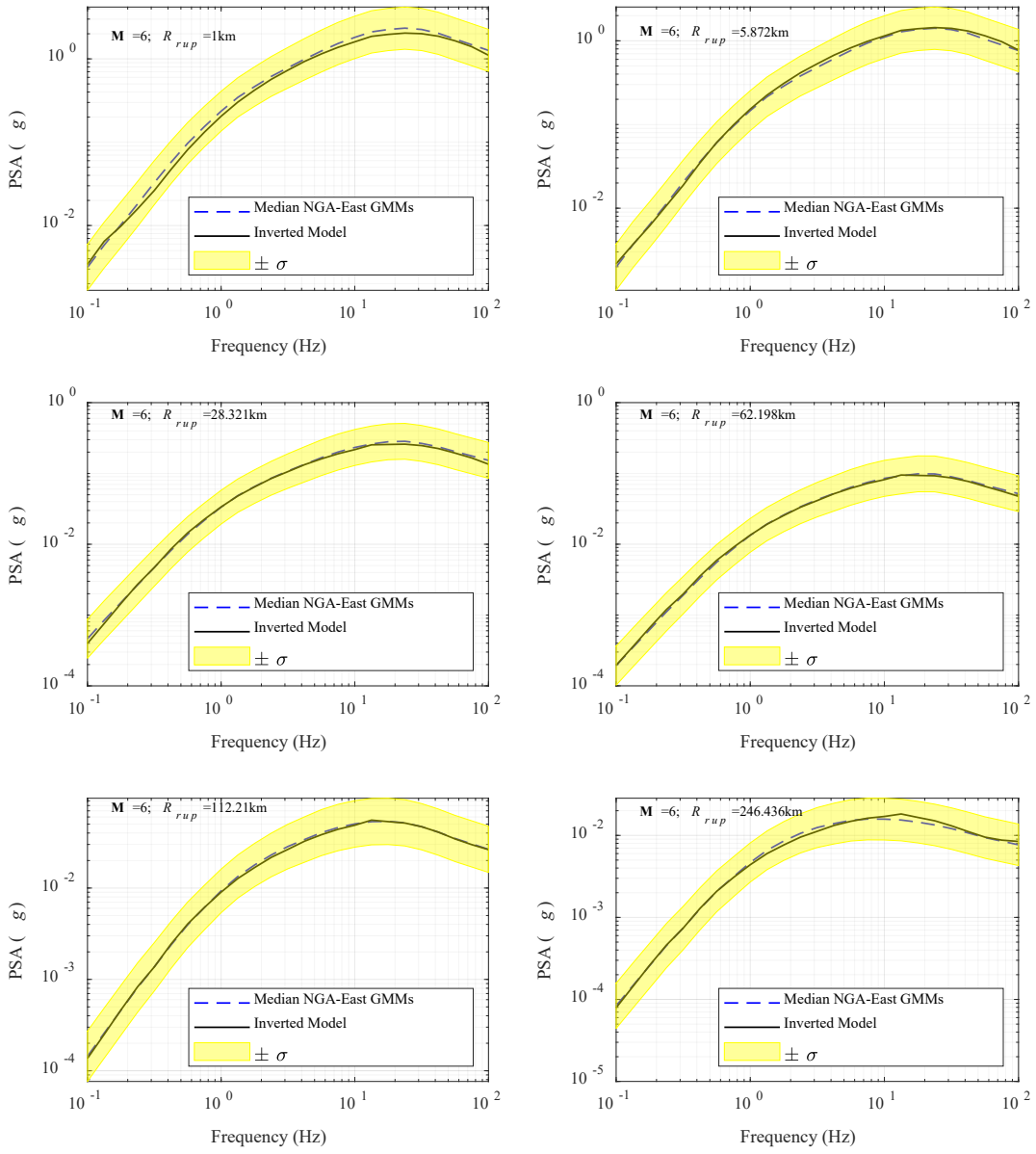

Figure 4-2. Comparison of the predicted response spectra from the median NGA-East GMMs with the predicted response spectra obtained from the model obtained from the GA inversion of the NGA-East GMMs for **M** 6. The highlighted area is the NGA-East GMM predictions ±σ, where σ is the standard deviation of the NGA-East model.

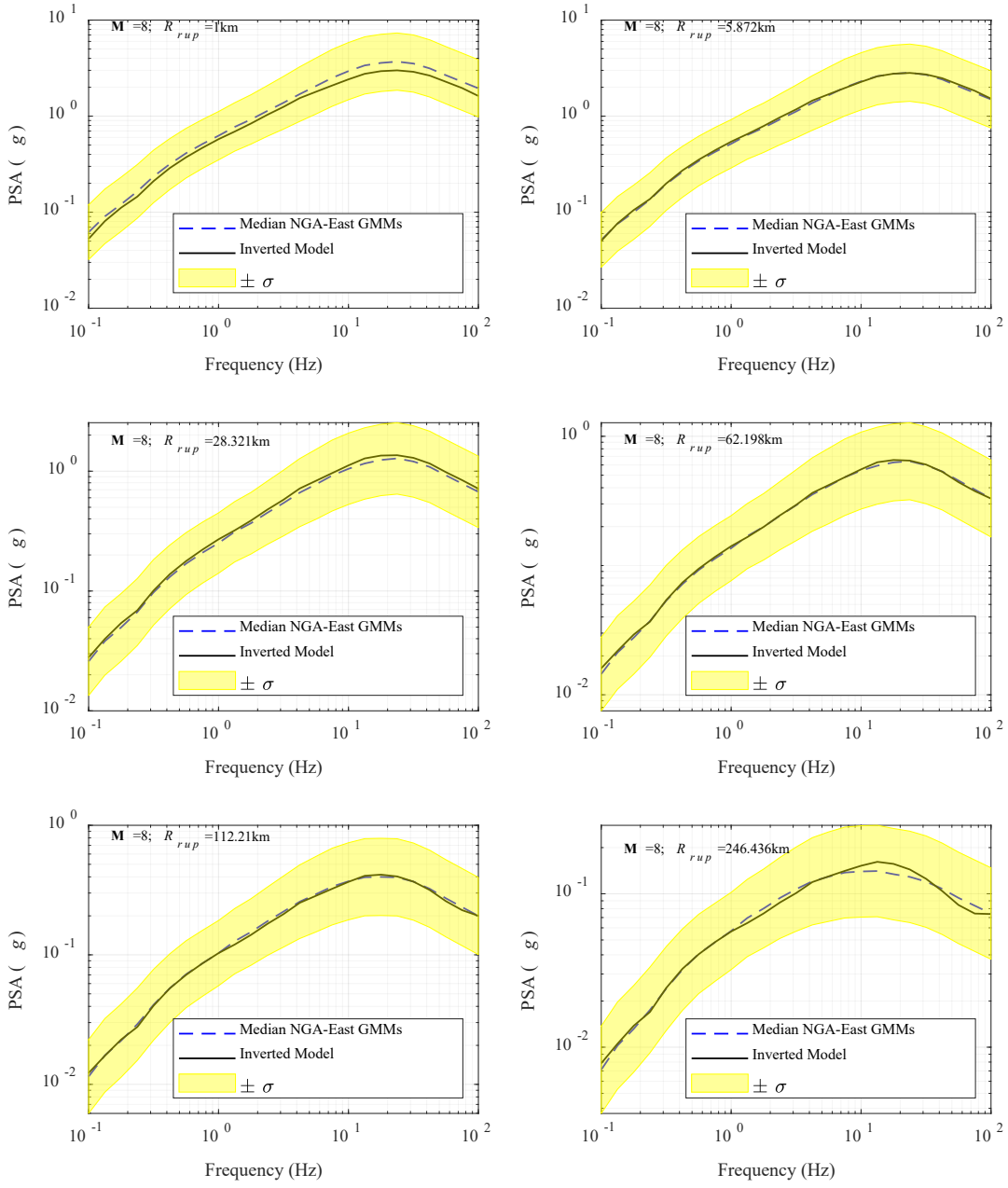

Figure 4-3. Comparison of the predicted response spectra from the median NGA-East GMMs with the predicted response spectra obtained from the model obtained from the GA inversion of the NGA-East GMMs for **M** 8. The highlighted area is the NGA-East GMM predictions ±σ, where σ is the standard deviation of the NGA-East model.

Figure 4-4 compares the magnitude scaling of Pseudo Spectral Acceleration (PSA) at 0.1, 1, 10, and 100 Hz for R_{RUP} 5.9, 10.6, 28.3, 62.2, 112.2, and 246.4 km for the median NGA-East GMMs and the inverted stochastic model. Figure 4-5 compares the distance scaling of PSA at 0.1, 1, 10, and 100 Hz for **M** 4, 5, 6, 7, and 8 for the median NGA-East GMMs and the inverted stochastic model. As can be seen in Figure 4-4 and Figure 4-5, the magnitude and distance scaling predicted by the stochastic model obtained in this study is in good agreement with those from NGA-East GMMs.

The misfit of the stochastic model with respect to the empirical GMMs is clearly seen in the residuals plotted in Figure 4-6 for the same magnitudes and distances used in Figure 4-3. These residuals, calculated from Equation (1), are defined as the difference between the logarithm base 10 of the predicted PSA of the empirical and stochastic models. In Figure 4-6 to Figure 4-8, lines indicating the ±10% and ±25% difference between the PSA values from the inverted stochastic model with respect to the median NGA-East GMMs are also plotted.

As shown in Figure 4-6, Figure 4-7, and Figure 4-8, predictions from the stochastic models are within 25% of the empirical model for many magnitudes, distances, and periods, except for R_{RUP} = 1 km for frequencies between 0.4 to 0.8 Hz for **M** 4. Figures 4-6 and 4-7 indicate that the stochastic model obtained in this study are in good agreement with NGA-East GMMs.

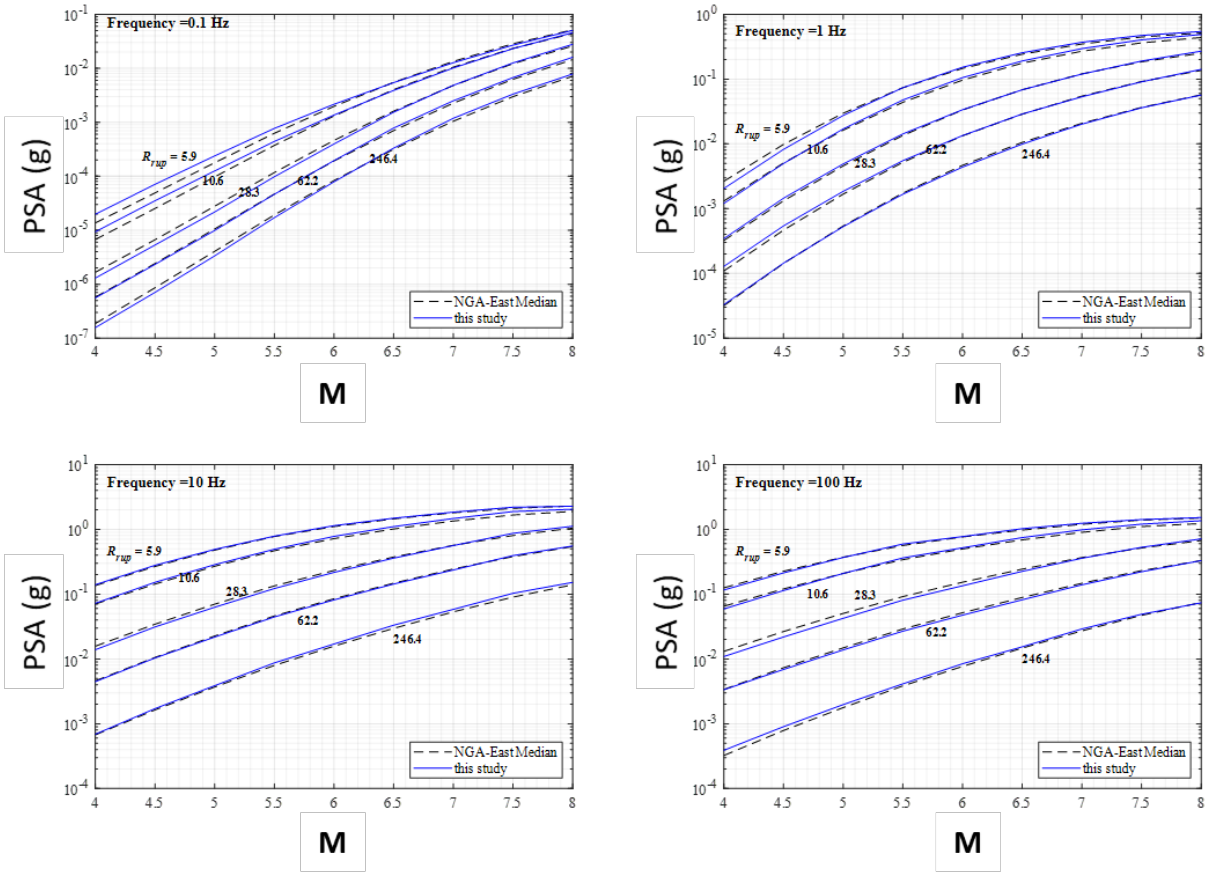

Figure 4-4. Comparison of predicted response spectra from the median NGA-East GMMs with the predicted response spectra obtained from the model obtained from the GA inversion of the NGA-East GMMs showing the magnitude scaling at f = 0.1, 1, 10, and 100 Hz.

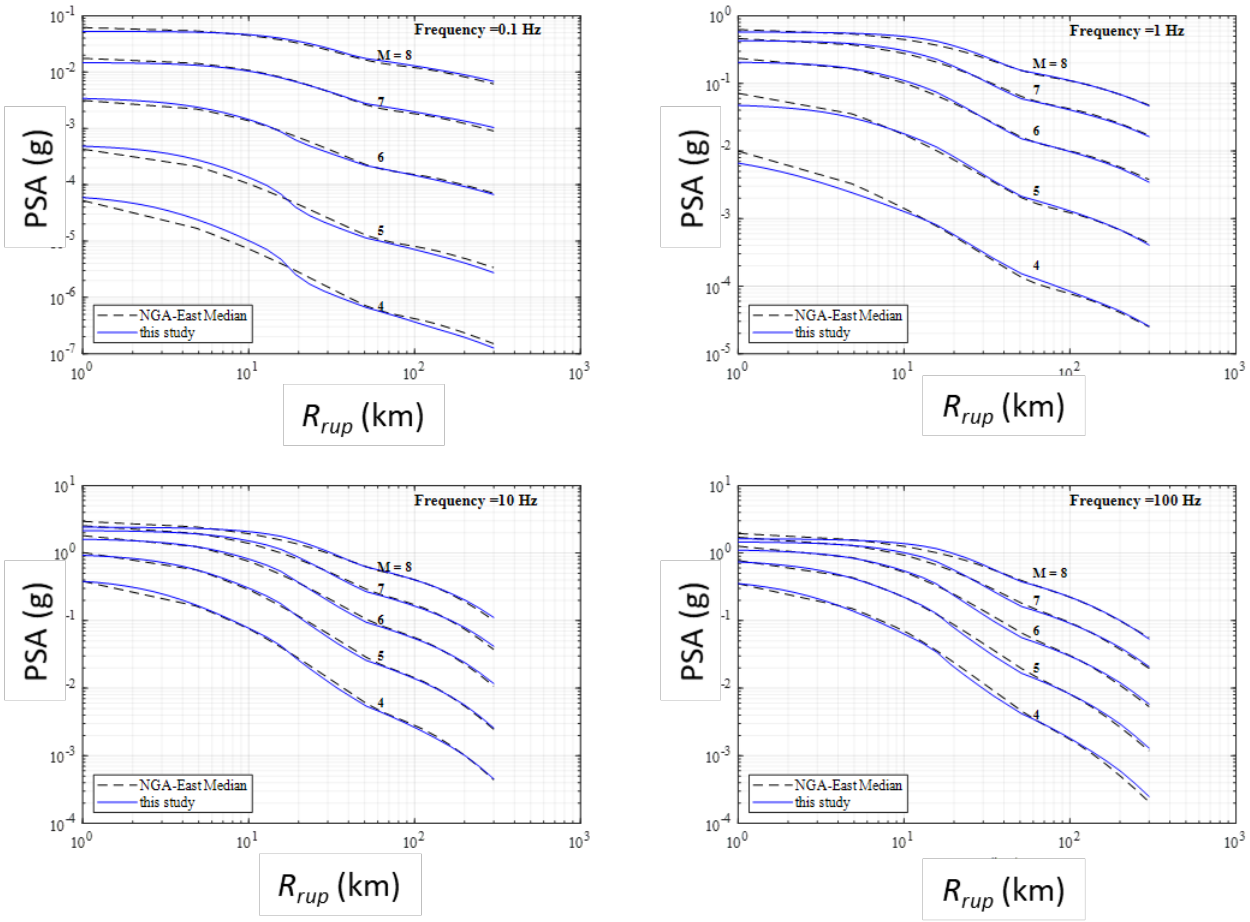

Figure 4-5. Comparison of predicted response spectra from the median NGA-East GMMs with the predicted response spectra obtained from the model obtained from the GA inversion of the NGA-East GMMs showing the distance scaling at f = 0.1, 1, 10, and 100 Hz.

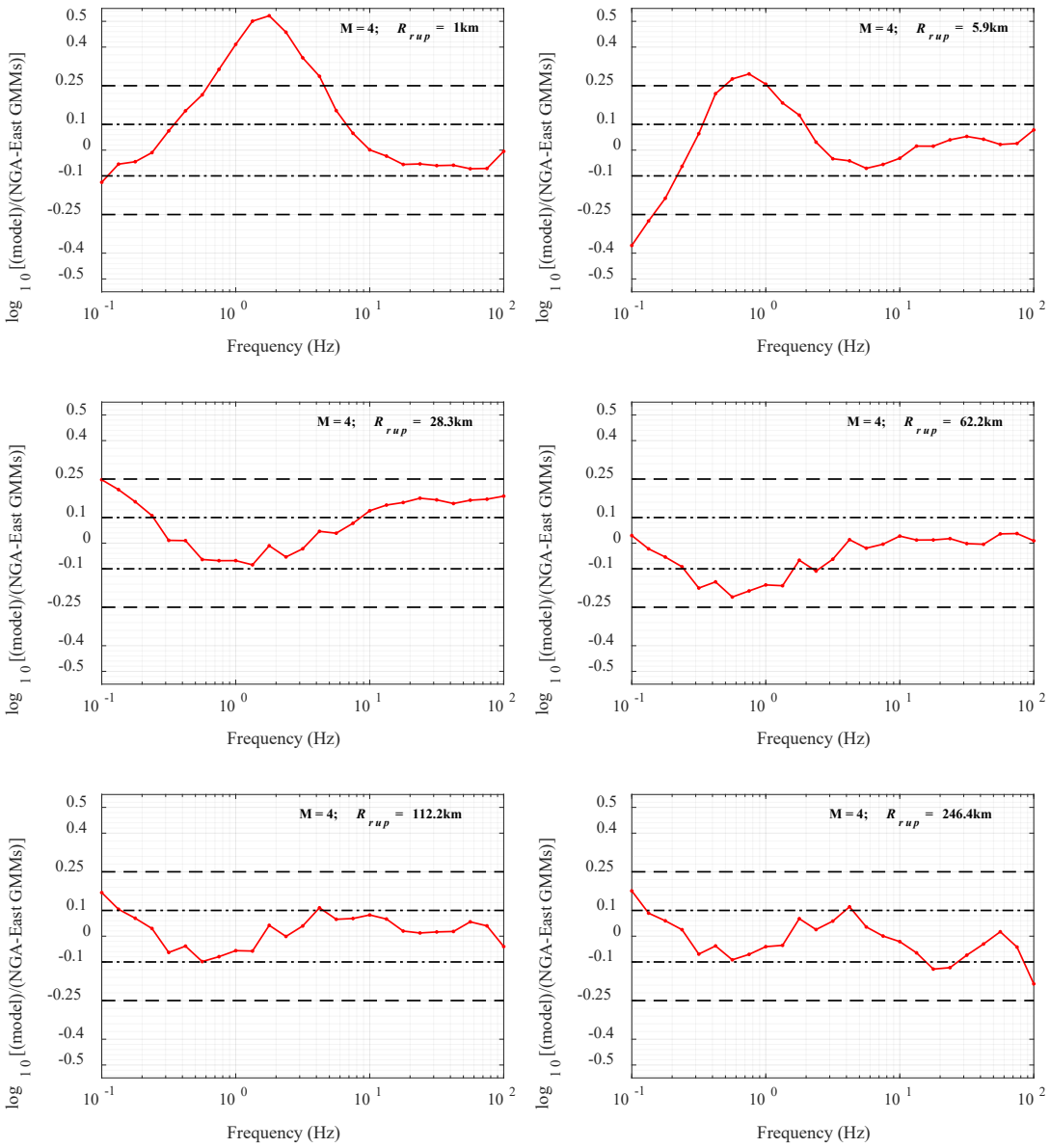

Figure 4-6. Plot of the residuals versus frequency between the predicted response spectra from the median NGA-East GMMs with the predicted response spectra obtained from the model obtained from the GA inversion of the NGA-East GMMs for **M** = 4. Note: When the residuals are positive, that means that the model is under-predicting and when the residuals are negative, the model is over-predicting the response.

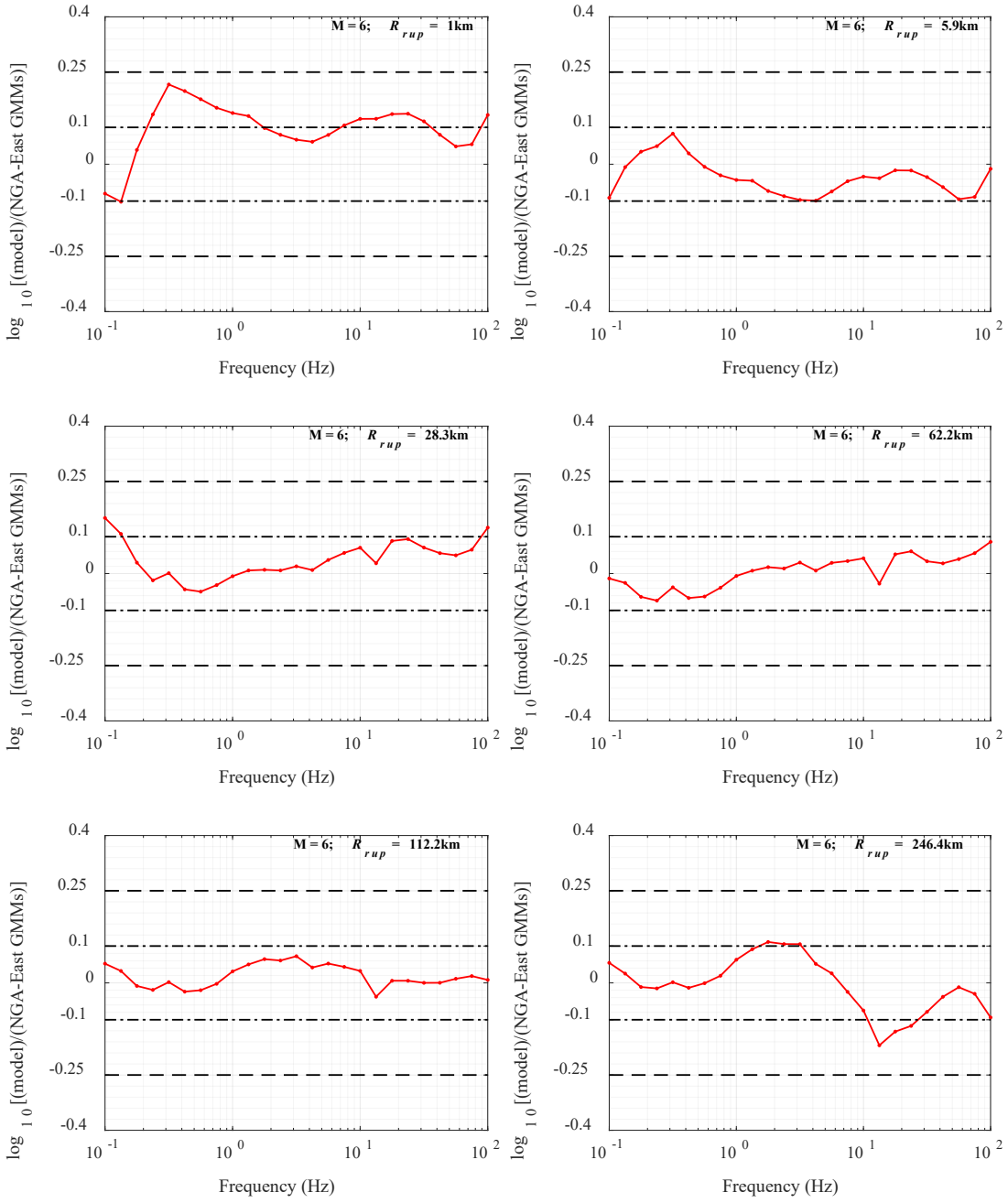

Figure 4-7. Plot of the residuals versus frequency between the predicted response spectra from the median NGA-East GMMs with the predicted response spectra obtained from the model obtained from the GA inversion of the NGA-East GMMs for **M** = 6. Note: When the residuals are positive, that means that the model is under-predicting and when the residuals are negative, the model is over-predicting the response.

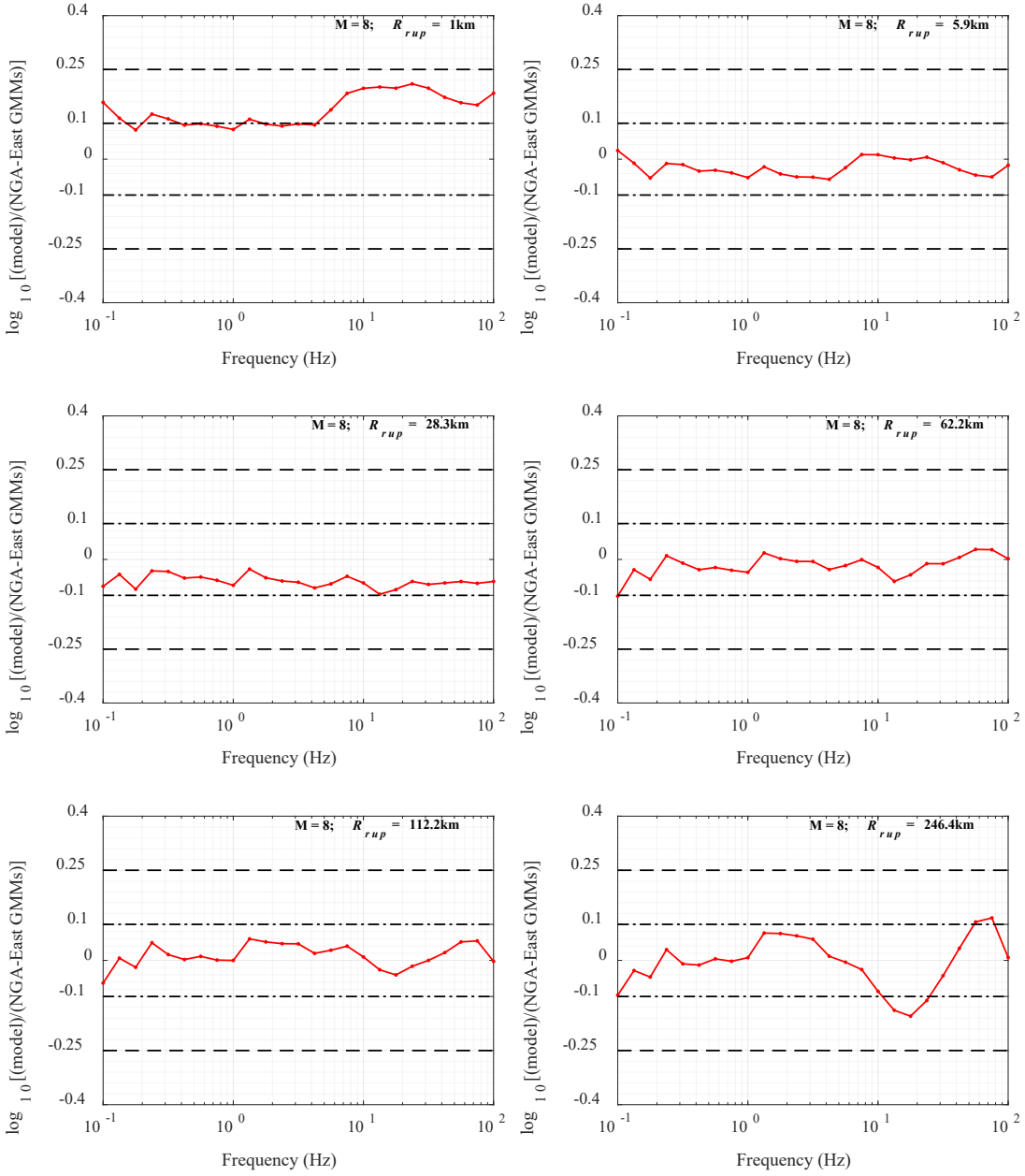

Figure 4-8. Plot of the residuals versus frequency between the predicted response spectra from the median NGA-East GMMs with the predicted response spectra obtained from the model obtained from the GA inversion of the NGA-East GMMs for **M** = 8. Note: When the residuals are positive, that means that the model is under-predicting and when the residuals are negative, the model is over-predicting the response.

Figure 4-9 depicts magnitude, frequency, and distance combinations for which the PSA values predicted from the inverted seismological point-source model are different from the median NGA-East GMM predictions by more than 25%. In general, differences larger than 25% are not detected at $f > 5$ Hz for the entire distance and magnitude ranges used in the inversion. In general, the maximum difference between the inverted model and the empirical model is less than 25%. Differences larger than 25% are not observed **M** 6 and higher. For **M** 4 to 5.5, there are cases with distances less than 10 km and frequencies less than 5 Hz that the differences are larger than 25% (but less than 40%) and are not considered to be of engineering interest.

Figure 4-10 shows magnitude, frequency, and distance combinations for which the ground motion estimates from the inverted point-source model are within 10% of the median NGA-East GMM predictions. From Figure 4-10, it can be observed that predictions from the inverted model are within 10% of the empirical model for the majority of magnitudes, distance, and frequencies used in the inversion. It can be observed that the inversion performs well. Information provided in Figures 4-9 and 4-10 shows that the inverted seismological parameters do a good job of predicting the ground motion models with a high level of accuracy.

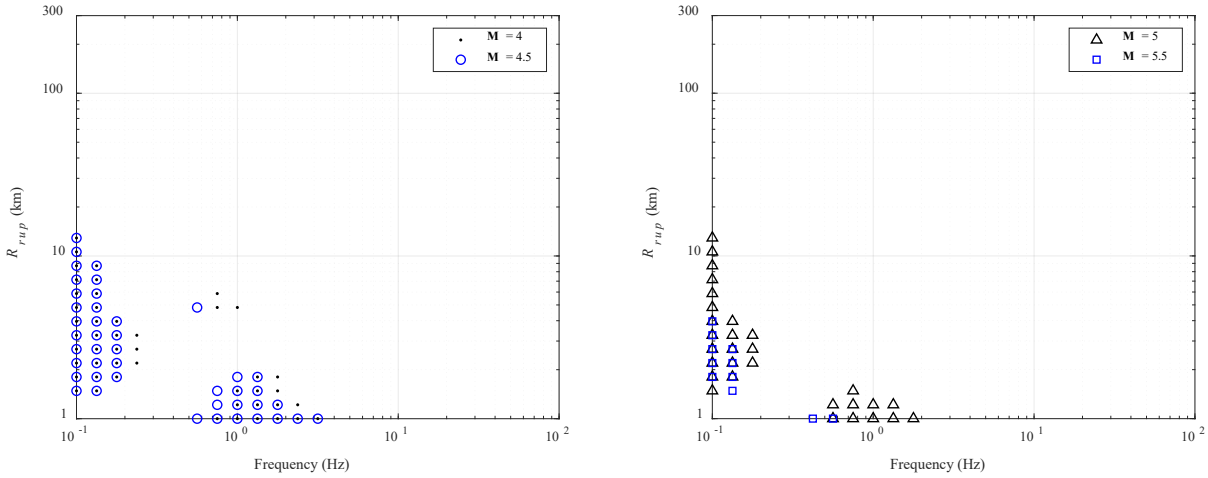

Figure 4-9. Frequency, magnitude, and distance combinations for which the PSA values predicted from the model obtained from the GA inversion of the NGA-East GMMs are different from the median NGA-East GMM predictions by more than 25%. There are no combinations that include M = 6, 6.5, 7, 7.5, or 8 that resulted in residuals greater than 25%.

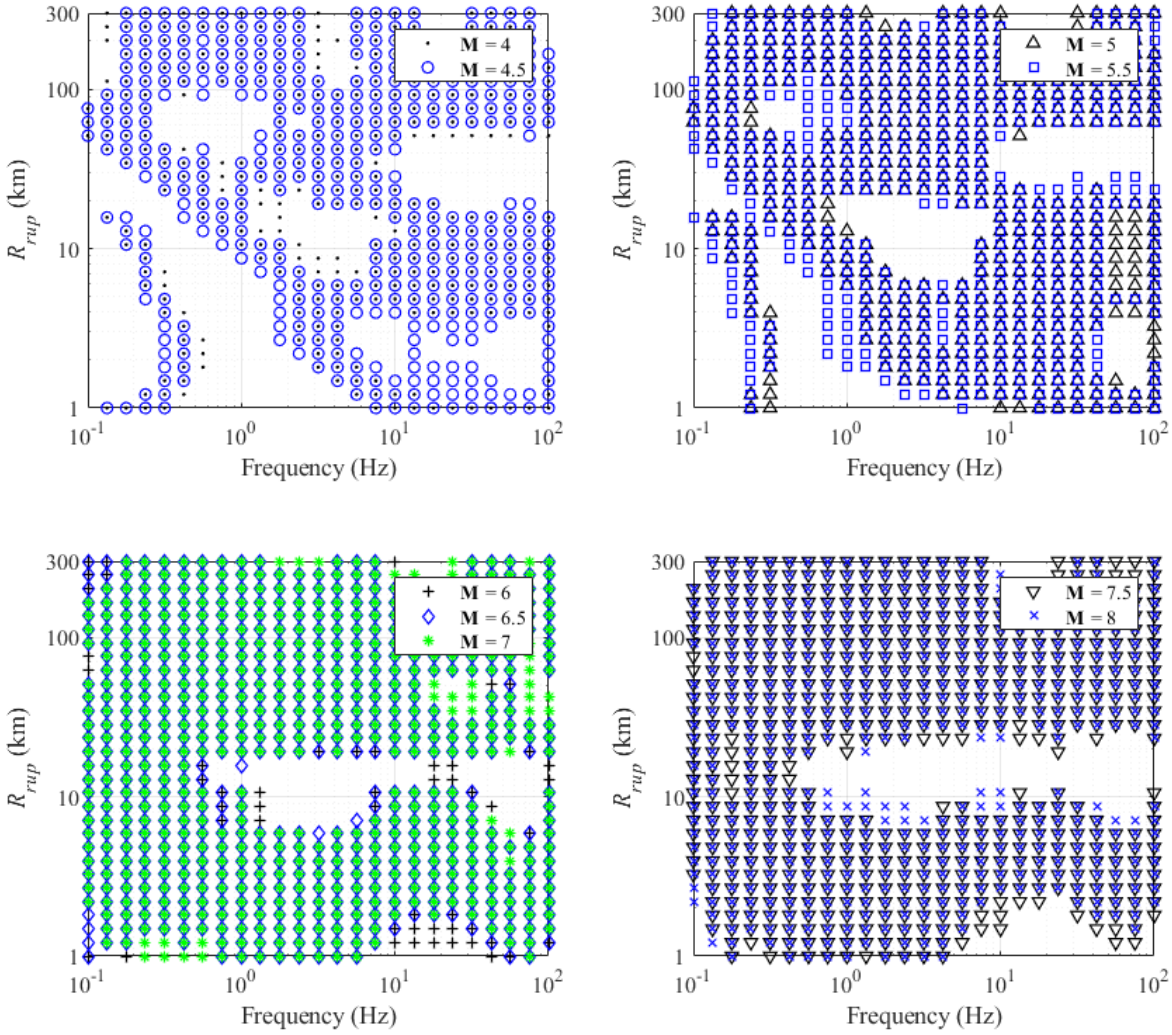

Figure 4-10. Frequency, magnitude, and distance combinations for which the PSA values predicted from the model obtained from the GA inversion of the NGA-East GMMs are different from the median NGA-East GMM predictions by less than 10%.

4.1 Near-Source Geometric Attenuation

Yenier and Atkinson (2015b) used to conclude that their best-fit bilinear simulation model suggests that the attenuation in Central and Eastern North America can be modeled with a distance decay of $R^{-1.3}$ within 50 km and $R^{-0.5}$ at further distances. They base this conclusion on their observation that the steeper near-source spreading does a better job at matching near-source attenuation trends than the traditional $R^{-1.0}$ model. Pezeshk *et al.* (2018) also used $R^{-1.3}$ within 60 km.

This study used a magnitude- and frequency-dependent near-source geometrical spreading coefficient b_1 and magnitude-dependent coefficients b_2 and b_3. Geometrical spreading coefficients obtained from the GA inversion are shown in Figure 3-2. A systemic trend in b_1 with magnitude and frequency can be observed in Figure 3-2. At low frequencies, b_1 has a general trend of decreasing for frequencies less than 0.2 Hz, and a general trend of increasing with higher frequencies. Coefficient b_2 increases with magnitude from about -0.745 at **M** 4.0 to about -0.409 at **M** 8.0. The coefficient b_3 ranges from -0.745 to 0.509 over this same magnitude range as shown in Figure 3-2. The coefficient b_3 obtained in the study is generally smaller than the value of -0.5 for **M** less than 6.5, which is typically attributed to the attenuation of L_g waves (e.g., Street et al., 1975). It should be noted that there is a trade-off between coefficients b_1, b_2, and b_3 obtained from the inversion. It is important to recognize this correlation when using or interpreting these results.

4.2 Effective depth

Yenier and Atkinson (2014) modeled the effective depth as log$h$(**M**) = –1.72+0.430**M** for moderate-to-large magnitude earthquakes. YA15 adopted the depth model of Atkinson and Silva (2000) expressed as log$h$(**M**) = –0.050+0.150**M** for **M** < 6 events and the relation by Yenier and Atkinson (2014) for **M** > 6 for a final model of log$h$(**M**) = max(–0.050+0.150**M,** –1.72+0.430**M**. YA15 also introduced an alternative model expressed as log$h$(**M**) = –0.405+0.235**M** to prevent oversaturation at close distances for large events and high frequencies in forward modeling. This latter model implies a depth of about 3 km at **M** 3.5 and about 30 km at **M** 8.

Pezeshk *et al.* (2018) modeled the effective depth as:

$$\log h = \begin{cases} \max(-0.05+0.15\mathbf{M}, -1.72+0.43\mathbf{M}) & \mathbf{M} \le 6.75 \\ -0.405+0.235\mathbf{M} & \mathbf{M} > 6.75 \end{cases} \quad (8)$$

The effective depth obtained in this study is shown in Figure 3-4. An exponential model of log$h$(**M**) = –0.409+0.207**M** is fitted to the depth values obtained from the inversion. The effective-depth values in this study increase from about 2.66 km at **M** 4 to about 17.66 km at **M** 8. It is similar to that by Pezeshk *et al*. (2018), which predicts a depth of about 3.43 km at **M** 4.0 and about 14.12 km at **M** 8.

It is important to note that the results for near-source geometrical spreading coefficients b_1 is correlated with the effective depth and our particular choice of the relationship used to convert

the value of R_{RUP} (used in the GMMs) to the equivalent point-source distance metric R_{PS} (used in the stochastic simulations).

4.3 Anelastic Attenuation

The anelastic attenuation parameters σ_0 and η have values that are strongly dependent on the geometric spreading coefficient at large distances, characterized by the parameters b_2 and especially b_3 in this study. For this study, we did not use a far-source geometric spreading coefficient of –0.5 consistent with the attenuation of L_g waves (e.g., Street et al., 1975) but instead obtained b_3 directly from the inversion. The anelastic attenuation parameters Q_0 and η obtained in this study are listed in Table IV. These parameter values, along with the quality factor function, $Q(f) = Q_0 f^{\eta}$ are shown in Figure 3-6. The values of Q_0 range from about 430 to 482 and those of η ranges from 0.573 to 0.649 for different magnitudes.

The anelastic attenuation parameters Q_0 and η have values that are strongly dependent on the geometric spreading coefficient at large distances, characterized by the parameters b_2 and especially b_3. For this study, we did not use a far-source geometric spreading coefficient of 0.6 consistent with the attenuation of L_g waves (e.g., Street et al., 1975) but instead obtained b_3 directly from the inversion. The anelastic attenuation parameters Q_0 and η obtained in this study are listed in Table IV. These parameter values, along with the quality factor function, $Q(f) = Q_0 f^{\eta}$ are shown in Figure 3-6. The values of Q_0 range from about 430 to 482 and those of η ranges from 0.573 to 0.649 for different magnitudes.

Chapman *et al.* (2014) derived Q_0 and η using recordings from the EarthScope Transportable Array (TA Array) and through an iterative inversion process, deriving a trilinear geometric attenuation model with $R^{-1.3}$ spreading to 60 km, R^{0} (or no spread) from 60 to 120 km, and $R^{-1.3}$ (or L_g) spreading beyond 120 km. At regional distances, the dominant phase in the ground-motion recording is the L_g phase, which is composed of multiple reflections of *S*-waves trapped within the crust. Chapman *et al.* (2014) found that for all CENA regions outside of the Gulf Coast region, the quality factor that is consistent with the above geometric attenuation term is given by the relationship $Q = 440\, f^{0.47}$, which is close to values obtained in this study.

Chapter 5 Summary and Discussion

We used a genetic algorithm (GA) to invert weighted geometric mean estimates of horizontal response-spectral acceleration from the empirical NGA-East GMMs to estimate a consistent set of seismological parameters that can be used along with an equivalent point-source stochastic model to mimic the general scaling characteristics of these GMMs. The inversion is performed for events of **M** 4 – 8.0, R_{RUP} = 1 to 300 km, T = 0.01 – 10 sec (f = 0.1 – 10 Hz), the CENA reference hard-rock site condition of V_{S30} = 3000 m/sec.

Several elements of the seismological model were fixed to values obtained in recent studies in the inversion to avoid non-convergence issues (Table I). These included the source-spectral shape (Brune 1971, 1972), the source velocity and source density (Boore, 2016), the geometric spreading transition distances for the geometrical spreading model (Boore and Thompson, 2015), the path duration (Boore and Thompson, 2015), and the site-amplification factors (Boore, 2016). All other parameters in Table I were fit in the inversion. The final results are summarized in Table IV for both the bilinear and trilinear geometric attenuation models.

One of the more interesting results of the inversion is the magnitude- and frequency-dependent near-source geometric spreading. The geometric spreading for $R_{RUP} \leq 50$ km is consistent with a distance decay of about $R^{-0.906}$ *to* $R^{-1.016}$ for **M** ranging from 4 to 8, at low frequencies of $f \leq 1$ Hz. In the vicinity of 1 Hz, b_1 converges to about $R^{-1.0}$ for all magnitudes, and in the vicinity of 20 Hz, it converges to $R^{-0.89}$ for all magnitudes. The stress parameter as a function of magnitude varies between 104 to 117.

The seismological parameters for the stochastic point source model obtained in this study are given in Tables I and IV. The parameters obtained from the GA inversion are provided in Table IV for the magnitudes used in the process. The near-source geometrical spreading coefficient b_1 is given as a function of frequency in addition to magnitude. For magnitudes other than those given in Table IV, parameters should be calculated by linear interpolation. For frequencies other than those given in Table IV, b_1 the parameter should be calculated by linear-log interpolation (log space for frequency).

Chapter 6 Conclusion

The purpose of this study was to estimate the seismological parameters (such as stress parameter, kappa, geometrical spreading, anelastic attenuation) to use with a stochastic point-source model for CENA from the NGA-East GMMs to obtain a set of parameters that are self-consistent and, thus, maintain the proper correlation between parameters. We used a genetic algorithm (GA) to perform a point-source inversion for events and sites with $R_{RUP} \leq 300$ km, for magnitudes **M** 4 to 8, the CENA reference hard-rock site condition of V_{S30} = 3000 m/sec. The derived model parameters were internally consistent and properly correlated, and suitable for use in developing stochastic and HEM-based GMMs for the CENA.

It is important to note that it has been 10 years since the start of the NGA-East. Since then, and since the publication of NGA-EAST GMMs (PEER 2015), there have been various advancements in site response for CENA, but there has not been any new research to improve the seismological parameters for CENA. This research will provide the much-needed information for future updating of GMMs developed as part of NGA-East in 2015.

While this study does not provide TDOT engineers with that which can be immediately implemented, it provides a significant impact on updating seismic hazard maps that will be developed by the United States Geological Survey (USGS). The American Associate of State Highway Transportation Officials (AASHTO) will use seismic hazard maps in future seismic design specifications and in turn, will be used by TDOT engineers for the future of the design of bridges in Tennessee. In summary, this research will provide accurate and science-based results that will be used to improve seismic hazard maps employed for the seismic design of bridges in Tennessee.

<u>Long-Term Implementation:</u>

While this study does not provide TDOT engineers with that can be immediately implemented, it provides a significant impact on updating seismic hazard maps that will be developed by the United States Geological Survey (USGS). American Associate of State Highway Transportation Officials (AASHTO) will use seismic hazard maps for the future seismic design specifications and, in turn, will be used by TDOT engineers to design bridges in Tennessee. In summary, this research will provide accurate and science-based results that will be used to improve seismic hazard maps employed for the seismic design of bridges in Tennessee.

<u>Immediate Recommendations:</u>

We recommend that our model provided in Supplement I: “A new model for vertical to horizontal response spectra for Central and Eastern North America” be used for developing the vertical response spectra for the design of bridges in Tennessee. Furthermore, the proposed model provided in Supplement II: “A ground-motion prediction model for small-to-moderate induced earthquakes for Central and Eastern United States,” could apply in long-term and short-term U.S. Geological Survey National Hazard maps for the hazard evaluation of induced seismicity in Tennessee. Finally, we propose using our model provided in Supplement III: “A ground-motion model for the Gulf Coast region of the United States,” be used for seismic design and assessment of bridges in West Tennessee.

References

1. The USC Libraries Guide on Writing Reports was used for our guidance. More information can be found here: https://www.hhs.gov/web/section-508/accessibility-checklists/index.html. (Note: This is not intended to be an example of a proper citation but for report guidance.)
2. Abrahamson, N. A., W. J. Silva, and R. Kamai (2014). Summary of the ASK14 ground motion relation for active crustal regions, *Earthq. Spectra* **30**, 1025–1055.
3. Anderson, J. G., and S. E. Hough (1984). A model for the shape of the Fourier amplitude spectrum of acceleration at high frequencies, *Bull. Seism. Soc. Am*. **74**, 1969–1993.
4. Atkinson, G. M. (2004). Empirical attenuation of ground motion spectral amplitudes in southeastern Canada and the northeastern United States, *Bull. Seismol. Soc. Am*. **94**, 1079–1095.
5. Atkinson, G. M. (2008). Ground motion prediction equations for eastern North America from a referenced empirical approach: Implications for epistemic uncertainty, *Bull. Seismol. Soc. Am*. **98**, 1304–1318.
1. Atkinson, G. M., and K. Assatourians (2010). Attenuation and source characteristics of the June 23 2010 **M** 5.0 Val-des-Bois, Quebec, earthquake, *Seismol. Res. Lett.* **81**, 849–860.
2. Atkinson, G. M., and D. M. Boore (1995). New ground motion relations for eastern North America, *Bull. Seismol. Soc. Am.* **85**, 17–30.
3. Atkinson, G. M., and D. M. Boore (1998). Evaluation of models for earthquake source spectra in eastern North America, *Bull. Seismol. Soc. Am*. **88**, 917–934.
4. Atkinson, G. M., and D. M. Boore (2006). Ground motion prediction equations for earthquakes in eastern North America, *Bull. Seismol. Soc. Am*. **96**, 2181–2205.
5. Atkinson, G. M., and D. M. Boore (2011). Modifications to existing ground-motion prediction equations in light of new data, *Bull. Seismol. Soc. Am*. **101**, 1121–1135.
6. Atkinson, G. M., and W. Silva (1997). An empirical study of earthquake source spectra for California earthquakes, *Bull. Seismol. Soc. Am*. **87**, 97–113.
7. Atkinson, G. M., and W. Silva (2000). Stochastic modeling of California ground motions, *Bull. Seismol. Soc. Am.* **90**, 255–274.
8. Atkinson, G. M., and D. J. Wald (2007). Did you feel it? Intensity data: A surprisingly good measure of earthquake ground motion, *Bull. Seismol. Soc. Am*. **78**, 362–368.
9. Atkinson, G. M., D. M. Boore, K. Assatourians, K. W. Campbell, and D. Motazedian (2009). A guide to differences between stochastic point-source and stochastic finite-fault simulations, *Bull. Seismol. Soc. Am.* **99**, 3192–3201.
10. Boore, D. M. (1983). Stochastic simulation of high-frequency ground motion based on seismological models of the radiated spectra, *Bull. Seismol. Soc. Am.* **73**, 1865–1893.
11. Boore, D. M. (2003). Prediction of ground motion using the stochastic method, *Pure Appl. Geophys.* **160**, 635–676.
12. Boore, D. M. (2005). SMSIM—Fortran Programs for Simulating Ground Motions from Earthquakes: Version 2.3–A Revision of OFR 96-80-A, *U.S. Geol. Surv. Open-File Rept. 00–509, Revised August 15 2005*, 55 pp.
13. Boore, D. M. (2009). Comparing stochastic point-source and finite-source ground-motion simulations: SMSIM and EXSIM, *Bull. Seismol. Soc. Am.* **99**, 3202–3216.

14. Boore, D. M. (2010). Orientation-independent, nongeometric-mean measures of seismic intensity from two horizontal components of motion, *Bull. Seismol. Soc. Am*. **100**, 1830–1835.
15. Boore, D. M. (2013). The uses and limitations of the square-root-impedance method for computing site amplification, *Bull. Seismol. Soc. Am.* **103**, 2356–2368.
16. Boore, D. M. (2015). *Adjusting Ground-Motion Intensity Measures to a Reference Site for which V_{S30}=3000 m/s, PEER Report 2015/06*, Pacific Earthquake Engineering Research Center, University of California, Berkeley, California, 85 pp.
17. Boore, D. M. (2016). Determining Generic Velocity and Density Models for Crustal Amplification Calculations, with an Update of the Boore and Joyner (1997) Generic Site Amplification for $V_S(Z)$=760 m/s, *Bull. Seismol. Soc. Am.* **106**, pp. 316–320.
18. Boore, D. M., and K. W. Campbell (2017). Adjusting central and eastern North America ground-motion intensity measures between sites with different reference-rock site conditions, *Bull. Seismol. Soc. Am.* **107**, 132–148.
19. Boore, D. M., and W. B. Joyner (1997). Site amplification for generic rock sites, *Bull. Seismol. Soc. Am*. **87**, 327–341.
20. Boore, D. M., and E. M. Thompson (2014). Path duration for use in the stochastic-method simulation of ground motions, *Bull. Seismol. Soc. Am.* **104**, 2541–2552.
21. Boore, D. M., and E. M. Thompson (2015). Revisions to some parameters used in stochastic method simulations of ground motion, *Bull. Seismol. Soc. Am.* **105**, submitted.
22. Boore, D. M., K. W. Campbell, and G. M. Atkinson (2010). Determination of stress parameters for eight well-recorded earthquakes in eastern North America, *Bull. Seismol. Soc. Am.* **100**, 1632–1645.
23. Boore, D. M., J. P. Stewart, E. Seyhan, and G. M. Atkinson (2014). NGA-West2 equations for predicting PGA, PGV, and 5% damped PSA for shallow crustal earthquakes, *Earthq. Spectra* **30**, 1057–1085.
24. Bozorgnia, Y., and 30 other authors (2014). NGA-West2 research project, *Earthq. Spectra* **30**, 973–987.
25. Brune, J. (1970). Tectonic stress and the spectra of seismic shear waves, *J. Geophys. Res*. **75**, 4997–5009.
26. Brune, J. (1971). *Correction*: Tectonic stress and the spectra of seismic shear waves, *J. Geophys. Res.* **76**, 5002.
27. Campbell, K. W. (2003). Prediction of strong ground motion using the hybrid empirical method and its use in the development of ground–motion (attenuation) relations in eastern North America, *Bull. Seismol. Soc. Am.* **93**, 1012–1033.
28. Campbell, K. W. (2007). *Validation and Update of Hybrid Empirical Ground Motion (Attenuation) Relations for the CEUS*, final report to U.S. Geological Survey, National Earthquake Hazards Reduction External Research Program, Award No. 05HQGR0032.
29. Campbell, K. W. (2008). Hybrid empirical ground motion model for PGA and 5% damped linear elastic response spectra from shallow crustal earthquakes in stable continental regions: Example for eastern North America. *Proc. 14th World Conference on Earthquake Engineering*, Oct. 12–17, Beijing, China, Paper No. S03-001.

30. Campbell, K. W. (2009). Estimates of shear-wave Q and κ_0 for unconsolidated and semiconsolidated sediments in eastern North America, *Bull. Seismol. Soc. Am*. **99**, 2365–2392.
31. Campbell, K. W. (2011). Ground motion simulation using the hybrid empirical method: Issues and insights, in *Earthquake Data in Engineering Seismology: Predictive Models, Data Management and Networks*, S. Akkar, P. Gulkan, and T. van Eck (eds.), Geotechnical, Geological and Earthquake Engineering Series, Vol. 14, Springer, London, pp. 81–95.
32. Campbell, K. W. (2014). An evaluation of eastern North America ground-motion models developed using the hybrid empirical method, *Bull. Seismol. Soc. Am.* **104**, 347–359.
33. Campbell, K. W., and Y. Bozorgnia (2008). NGA ground motion model for the geometric mean horizontal component of PGA, PGV, PGD and 5% damped linear-elastic response spectra for periods ranging from 0.01 to 10.0 s, *Earthq. Spectra* **24**, 139–171.
34. Campbell, K. W., and Y. Bozorgnia (2014). NGA-West2 ground motion model for the average horizontal components of PGA, PGV, and 5% damped linear acceleration response spectra, *Earthq. Spectra* **30**, 1087–1115.
35. Campbell, K. W., Y. M. A. Hashash, B. Kim, A. R. Kottke, E. M. Rathje, W. J. Silva, and J. P. Stewart (2014). *Reference Rock Site Conditions for Central and Eastern North America: Part II – Attenuation (Kappa) Definition*, PEER Report No. 2014/12, Pacific Earthquake Engineering Research Center, University of California, Berkeley, CA, 54 pp.
36. Chapman, M., S. Pezeshk, M. Hosseini, and A. Conn (2014). Regional study of Fourier amplitude drop of *Lg*-wave acceleration in central United States, *Seismol. Res. Lett*. **85**, 513.
37. Chiou, B. S.-J., and R. R. Youngs (2014). Update of the Chiou and Youngs NGA model for the average horizontal component of peak ground motion and response spectra, *Earthq. Spectra* **30**, 1117–1153.
38. Douglas, J. (2003). Earthquake ground motion estimation using strong-motion records: A review of equations for the estimation of peak ground acceleration and response spectral ordinates, *Earth-Sci. Rev.* **61**, 43–104.
39. Douglas, J. (2011). *Ground-Motion Prediction Equations, 1964–2010*, PEER Report No. 2011/102, Pacific Earthquake Engineering Research Center, University of California, Berkeley, CA. (updates available online at http://www.gmpe.org.uk.).
40. Douglas, J., H. Bungum, and F. Scherbaum (2006). Ground-motion prediction equations for southern Spain and southern Norway obtained using the composite model perspective, *J. Earthq. Eng.* **10**, 33–72.
41. Dreiling J., M. P. Isken, W. D. Mooney, M. C. Chapman, and R. W. Godbee (2014). *NGA-East Regionalization Report: Comparison of Four Crustal Regions within Central and Eastern North America Using Waveform Modeling and 5%-Damped Pseudo-Spectral Acceleration Response*, PEER Report No. 2014/15, Pacific Earthquake Engineering Research Center, University of California, Berkeley, CA.
42. Frankel, A., C. Mueller, T. Barnhard, D. Perkins, E. Leyendecker, N. Dickman, S. Hanson, and M. Hopper (1996). National seismic hazard maps: Documentation June 1996, *U.S. Geol. Surv. Open-File Rept. 96-532*, 110 pp.
43. Goldberg, D. E. (1989). Genetic Algorithms in Search, Optimization, and Machine Learning, Addison-Wesley, Reading, Massachusetts.

44. Goulet, C. A., T. Kishida, T. D. Ancheta, C. H. Cramer, R. B. Darragh, W. J. Silva, Y. M. A. Hashash, J. Harmon, J. P. Stewart, K. E. Wooddell, and R. R. Youngs (2014). *PEER NGA-East Database*, PEER Report No. 2014/17*,* Pacific Earthquake Engineering Research Center, University of California, Berkeley, CA.
45. Goulet, C. A., Y. Bozorgnia, N. Abrahamson, N. Kuehn, L. Al Atik, R. Youngs, R. Graves, G. Atkinson (2018). Central and Eastern North America Ground-Motion Characterization, PEER Report No. 2018/08*,* Pacific Earthquake Engineering Research Center, University of California, Berkeley, CA.
46. Hanks, T. C. (1982). f_{max}, *Bull. Seismol. Soc. Am*. **72**, 1867–1879.
47. Hanks, T. C., and R. K. McGuire (1981). The character of high–frequency strong ground motion, *Bull. Seismol. Soc. Am*. **71**, 2071–2095.
48. Harmon, J. A., Y. M. A. Hashash, J. P. Stewart, E. M. Rathje, K. W. Campbell, W. J. Silva, and O. Ilhan (2019). Site Amplification Functions for Central and Eastern North America – Part II: Modular Simulation-Based Models, *Earthquake Spectra*, **35**(2), p. 815–847.
49. Hashash, Y. M. A., A. R. Kottke, J. P. Stewart, K. W. Campbell, B. Kim, C. Moss, S. Nikolaou, E. M. Rathje, and W. J. Silva (2014a). Reference rock site condition for central and eastern North America, *Bull. Seismol. Soc. Am*. **104**, 684–701.
50. Hashash, Y. M. A., A. R. Kottke, J. P. Stewart, K. W. Campbell, B. Kim, E. M. Rathje, and W. J. Silva, S. Nikolaou, and C. Moss (2014b). *Reference-Rock Site Conditions for Central and Eastern North America: Part I – Velocity Definition*, PEER Report No. 2014/11, Pacific Earthquake Engineering Research Center, University of California, Berkeley, CA, 154 pp.
51. Hashash, Y. M., I. Okan, J. A. Harmon, G. A. Parker, J. P. Stewart, E. M. Rathje, K. W. Campbell, and W. J. Silva (2020). Nonlinear site amplification model for ergodic seismic hazard analysis in Central and Eastern North America. *Earthquake Spectra*, **36**(1), pp. 69–86. doi: 10.1177/8755293019878193.
52. Hassani, B., and G. M. Atkinson (2015). Referenced empirical ground-motion model for eastern North America, *Seismol. Res. Lett.,* **86**, 477–491.
53. Hough, S. E. (2014). Shaking from injection-induced earthquakes in the central and eastern United States, *Bull. Seismol. Soc. Am*. **104**, 2619–2626.
54. Holland, J. H. (1975). Adaptation in Natural and Artificial Systems, The University of Michigan Press, Ann Arbor, Michigan.
55. Kottke, A. R., and E. M. Rathje (2008). *Technical Manual for Strata*, PEER Report No. 2008/10, Pacific Earthquake Engineering Research Center, University of California, Berkeley, CA.
56. Ktenidou, O. J., F. Cotton, N. A. Abrahamson, and J. G. Anderson (2014). Taxonomy of κ: A review of definitions and estimation approaches targeted to applications, *Seismol. Res. Lett*. **85**, 135–146.
57. Idriss, I. M. (2014). An NGA-West2 empirical model for estimating the horizontal spectral values generated by shallow crustal earthquakes, *Bull. Seismol. Soc. Am*. **30**, 1155–1177.
58. McGuire, R. K., and T. C. Hanks (1980). RMS accelerations and spectral amplitudes of strong ground motion during the San Fernando, California, earthquake, *Bull. Seismol. Soc. Am*. **70**, 1907–1919.
59. Motazedian, D., and G. M. Atkinson (2005). Stochastic finite-fault modeling based on a dynamic corner frequency, *Bull. Seismol. Soc. Am*. **95**, 995–1010.

60. Parker, G. A. J. P. Stewart, Y. M. A. Hashash, E. M. Rathje, K. W. Campbell, W. J. Silva, and J. Harmon (2016). Empirical seismic site amplification in central and eastern North America from NGA-East ground motion database, Abstract, *Seismol. Res. Lett*. **87**, 555.
61. Parker, G. A., J. A. Harmon, J. P. Stewart, Y. M. A. Hashash, A. R. Kottke, E. M. Rathje, W. J. Silva, and K. W. Campbell (2017a). Proxy-based V_{S30} estimation in Central and Eastern North America, *Bull. Seismol. Soc. Am*. **107**, 117–131.
62. Parker, G. A., J. P. Stewart, J. A. Harmon, Y. M. A. Hashash, G. M. Atkinson, D. M. Boore, Y. Bozorgnia, R. Darragh, W. J. Silva (2017b). Recommended Central and Eastern North America Seismic Site Amplification Models for USGS Map Applications, SSA Annual Meeting, April 18-20, Denver, CO.
63. PEER (2015). *NGA-East: Median Ground Motion Models for the Central and Eastern North America Region*, PEER Report No. 2015/04, Pacific Earthquake Engineering Research Center, University of California, Berkeley, CA.
64. Pezeshk, S., A. Zandieh, and B. Tavakoli (2011). Hybrid empirical ground-motion prediction equations for eastern North America using NGA models and updated seismological parameters, *Bull. Seismol. Soc. Am*. **101**, 1859–1870.
65. Pezeshk, S., A. Zandieh, K. W. Campbell, and B. Tavakoli (2015). Ground-motion prediction equations for CENA using the Hybrid Empirical Method in Conjunction with NGA-West2 Empirical Ground-Motion Models, Chapter 5, PEER Report No. 2015/04.
66. Pezeshk, S., A. Zandieh, K. W. Campbell, and B. Tavakoli (2018). Ground-motion prediction equations for CENA using the Hybrid Empirical Method in Conjunction with NGA-West2 Empirical Ground-Motion Models, *Bull. Seismol. Soc. Am*., in press.
67. Scherbaum, F., J. J. Bommer, H. Bungum, F. Cotton, and N. A. Abrahamson (2005). Composite ground-motion models and logic trees: Methodology, sensitivities, and uncertainties, *Bull. Seismol. Soc. Am.* **95**, 1575–1593.
68. Scherbaum, F., F. Cotton, and H. Staektke (2006). The estimation of minimum-misfit stochastic model from empirical ground-motion prediction equations, *Bull. Seismol. Soc. Am.* **96**, , 417–445.
69. Silva, W., N. Gregor, and R. Darragh (2002). *Development of Regional Hard Rock Attenuation Relations for Central and Eastern North America*, Technical Report, Pacific Engineering & Analysis, El Cerrito, CA, 57 pp.
70. Stewart, J. P., G. A. Parker, J. P. Harmon, G. M. Atkinson, D. M. Boore, R. B. Darragh, W. J. Silva, and Y. M. A. Hashash (2017). Expert Panel Recommendations for Ergodic Site Amplification in Central and Eastern North America, *PEER 2017/04.*
71. Stewart, J. P., G. A. Parker, G. M., Atkinson, D. M., Boore, Y. M. A. Hashash, and W. J. Silva (2020). Ergodic site amplification model for central and eastern North America. *Earthquake Spectra*, **36**(1), pp. 42–68. doi: 10.1177/8755293019878185.
72. Tavakoli, B., and S. Pezeshk (2005). Empirical-stochastic ground-motion prediction for eastern North America, *Bull. Seismol. Soc. Am*. **95**, 2283–2296.
73. Toro, G. R., N. A. Abrahamson, and J. F. Schneider (1997). Model of strong ground motions from earthquakes in central and eastern North America: Best estimates and uncertainties*, Seismol. Res. Lett.* **68**, 41–57.

74. Yenier, E., and G. M. Atkinson (2014). Equivalent point-source modeling of moderate to large magnitude earthquakes and associated ground-motion saturation effects, *Bull. Seismol. Soc. Am*. **104**, 1458–1478.
75. Yenier, E., and G. M. Atkinson (2015a). Regionally-adjustable generic ground-motion prediction equation based on equivalent point-source simulations: Application to central and eastern North America, *Bull. Seismol. Soc. Am*., **105**, pp.1989–2009.
76. Yenier, E., and G. M. Atkinson (2015b). An equivalent point-source model for stochastic simulation of earthquake ground motions in California, *Bull. Seismol. Soc. Am*., **105**, pp.1435-1455.
77. Zandieh, A., K. W. Campbell, and S. Pezeshk (2016). Estimation of κ_0 implied by the high-frequency shape of the NGA-West2 ground motion prediction equations, *Bull. Seismol. Soc. Am*. **106**, *pp.1342–1356.*
78. Zandieh, A., S. Pezeshk, and K. W. Campbell (2018). The estimation of seismological parameters for use in a stochastic point source model for western United States using an inversion technique to match the median NGA-East GMMs, *Bull. Seismol. Soc. Am*., **108**(2), pp. 815–835.

Supplements

Supplement I. Published Paper: A New Model for Vertical to Horizontal Response Spectral Ratios for Central and Eastern North America

Abstract

It is a well-known fact that critical structures are required to be designed for the vertical effects of earthquake ground motions as well as the horizontal effects. We developed a new model for the spectral ratio of vertical to horizontal components of earthquakes (V/H ratio) for Central and Eastern North America (CENA). The proposed V/H ratio model has the advantage of considering the earthquake magnitude, source to site distance, and the shear-wave velocity of soil deposits in the upper 30*m* of the site for Peak Ground Acceleration (PGA) and a wide range of spectral periods (0.01 to 10.0 seconds). The model evaluation is based on a comprehensive set of regression analyses of the compiled Next Generation Attenuation (NGA-East) database of available CENA recordings with M ≥ 3.4 and R_{RUP} < 1000 km.

The median value of the geometric mean of the orthogonal horizontal motions rotated through all possible nonredundant rotation angles, known as the RotD50, is used along with the vertical component to perform regression using the nonlinear mixed-effects regression. We excluded the earthquakes and recording stations in the Gulf Coast region due to their different ground-motion attenuation (Dreiling *et al.*, 2014). To compute V/H ratios for the Gulf Coast region, we refer the readers to the study of Haji-Soltani *et al.* (2017). Moreover, we excluded the NEHRP site class E sites from consideration because of their complex site-response characteristics and their potential for nonlinear site effects. The predicted V/H ratios from the proposed model are compared with recently published V/H ratio models. We suggest our model be used for developing the vertical response spectra for CENA sites.

Supplement II. Published Paper: A ground-motion prediction model for small-to-moderate induced earthquakes for Central and Eastern United States

Abstract

This study presents a new ground motion model (GMM) for small-to-moderate potentially induced earthquakes for Central and Eastern United States (CEUS). We used a hybrid empirical model as the base model, which was developed and calibrated for tectonic events in Central and Eastern North America (CENA) as part of the Next-generation Attenuation-East (NGA-East) project. We calibrated the base model using a comprehensive database of potentially induced ground motions with smaller magnitudes and shallower depths than tectonic earthquakes, excluding all earthquake events and stations within the Gulf Coast region.

We determined the model functional form coefficients using a mixed-effect regression procedure. The proposed GMM is derived for the peak ground acceleration and response-spectral ordinates at periods ranging from 0.01 to 10.0s, moment magnitudes ranging from 3.0 to 5.8, and hypocentral distances up to 200km. The performance of the proposed GMM is evaluated through a set of comprehensive residual analyses. Furthermore, we compared the proposed GMM with recently published GMMs with the observed data for CEUS. The proposed GMM could apply in long-term and the short-term U.S. Geological Survey National Seismic Hazard Maps and for the hazard evaluation of induced seismicity.

Supplement III. Published Paper: A ground-motion model for the Gulf Coast Region of the United States

Abstract

In this study, the hybrid empirical method (HEM) was used to develop a new ground motion model (GMM) for the Gulf Coast of the United States. We used five new empirical GMMs developed by the Pacific Earthquake Engineering Research Center for the Next Generation Attenuation-West2 project to estimate ground-motion intensity measures (GMIMs) in the host region. The new GMM is derived for the horizontal peak ground acceleration and response-spectral ordinates at periods ranging from 0.01 to 10 s, moment magnitudes ranging from **M** 3.5 to 8.0, and rupture distance (R_{RUP}) as far as 1000 km from the site, although the GMMs are the best constrained for R_{RUP} < 300–400 km. The predicted GMIMs are for a reference site defined as the Gulf Coast region hard rock with V_{S30} = 3000 m/s and kappa_0 =0.006 s, in which V_{S30} is the time-averaged shear-wave velocity in the top 30 m of the site profile, and .0 is the total attenuation of the ground motion as it propagates through the site profile. Seismological parameters used to derive the GMIM stochastic estimates in the Gulf Coast target region are adopted from the most recent research and published information for the region. The seismological parameters for the western North America host region are adopted from Zandieh *et al*. (2017). The proposed GMM is compared with the Pezeshk et al. (2018) model, which is also a HEM approach, and was developed for central North America and excluded the Gulf Coast region to show the differences between the region.